UNIVERSITY OF CALIFORNIA, SAN DIEGO

Automation in Image Cytometry: Continuous HCS and Kinetic Image Cytometry

A dissertation submitted in partial satisfaction of the requirements of the degree
Doctor of Philosophy

in

Bioengineering

by

David J. Charlot

Committee in Charge:

David Gough, Chair
Michael Berns
Michael Heller
Mark Mercola
Jeffrey H. Price
John Watson

2012

The dissertation of David J. Charlot is approved, and it is acceptable in quality and form for publication on microfilm and electronically:

Chair

University of California, San Diego

2012

Dedication

This dissertation is dedicated to my Family, Fiancée, Friends, and the world of High Content Screening. Without you all, I would have contrast but no resolution, objective but no focus, and a light path but no Koehler illumination. Thank God.

Table of Contents

Section II - Kinectic Image Cytometry

List of Figures

Section I - Implementation of Continuous High Content Screening (HCS)

Section II - Kinectic Image Cytometry

List of Tables

Section I - Implementation of Continuous High Content Screening (HCS)

Section II - Kinectic Image Cytometry

Vita

2004 B. S., Physics with Medical Emphasis, Delaware State University

2005-2006 Graduate Teaching Assistant, University of California, San Diego

2006 M. S., Bioengineering, University of California, San Diego

2007-2010 Graduate Research Assistant, Sanford-Burnham Medical Research Institute

2012 Ph. D., Bioengineering, University of California, San Diego

Publications

1. Exact analytical and numerical calculation of the radiative recombination cross-sections of fully stripped ions. Zerrad E., Charlot D., Hahn Y., Journal of Electromagnetic Waves and Applications, Volume 20, Number 11, 2006, pp. 1495-1501(7)

2. Automated Calcium Measurements in Live Cardiomyocytes. Charlot D., Campa V., Azimi B., Mercola M., Ingermanson R., McDonough P.M., Price J.H., 2008 5th IEEE International Symposium on Biomedical Imaging: From Nano to Macro, Proceedings, ISBI, art. no. 4540996:316-319.

Patents

2010 Automated Transient Image Cytometry, Application No: 12/454,217 Publication No: US 2010/0289887 A1

Presentations

2007 Cytometry Development Workshop: *HTS Image Cytometry*

2008 Cytometry Development Workshop: *Calcium Transient Monitoring in HT environment*

2008 International Society for Analytical Cytology (ISAC) XXIV International Congress: *Implementation of High Throughput High Content Screening (HT-HCS) Using Time Delay and Integrate (Tdi) CCD Imaging and Dynamic Autofocus*

Honors

2003-2004 Minority Access to Research Careers (MARC) Scholar

Abstract of Dissertation

Automation in Image Cytometry: Continuous HCS and Kinetic Image Cytometry

By

David J. Charlot

Doctor of Philosophy in Bioengineering

University of California, San Diego, 2012

Professor David Gough, Chair

Image based high content analysis (HCA) and high content screens (HCS) are powerful tools used predominately in the study of cellular and molecular dynamics, function, and structure and for cDNA, RNAi and compound library screens. Analyses and screens based on fully automated image cytometry create a vast wealth of information in a hands free, unbiased manner. Large-scale screens of tens of thousands to millions of compounds and potential clinical diagnostic applications would benefit from increased image acquisition speeds.

Section I of this dissertation (Chapters 1-6) discusses the development of an HT-HCS instrument that uses TDI image capture and dynamic autofocus. Current

instruments typically scan at peak speeds of 20,000 to 50,000 wells/day (1-4 image(s)/well), whereas many define “high throughput” screening as > 100,000 wells/day. Progress is reported about routine continuous scanning with time-delay-and-integrate (TDI) 3-color fluorescence imaging at ~70,000 wells/day (20x 0.75 NA Nikon objective, 384-well plate, 8-10 usable images/well depending on wall thickness and edge effects). Image cytometry quality (e.g., precision, accuracy and dynamic range of measurements) is directly linked to the contrast and resolution (detail) available in each image, and is thus dependent on the quality of autofocus. The system was validated using a synthetic assay and compared with the Perkin Elmer Opera using an assay screened by the Sanford-Burnham Center for Chemical Genomics (Chapter 4).

Section II of this dissertation discusses the development of an HCS instrument capable of automatically stimulating, monitoring, and analyzing kinetic activity in cells. The Kinetic Image Cytometer or KIC will electrically stimulate (or pace) the cells, record the resulting Ca^{++} transients from cells in microtiter plates (e.g., with 96 wells), and automatically quantify characteristics such as the duration of the Ca^{++} waves on a cell-by-cell basis in a fully automated manner on large scale screens. Chapters 1 and 2 are a summation of research to develop the technology using cardiomyoctes as the control model. Chapters 3 and 4 are a summation of research to use the KIC to perform dose response assays of different chemical compounds on human cardiomyocytes from different sources, including hESC---derived cardiomyocytes (hESC---CMs) and hiPSC---derived cardiomyocytes (hiPSC---CMs).

Section I - Implementation of Continuous High Content Screening (HCS)

Chapter 1: High Content Screening

1.1 Introduction

Image based high content analysis (HCA) and high content screens (HCS) are powerful tools used predominately in the study of cellular and molecular dynamics, function, and structure; and also for cDNA, RNAi and compound library screens. Analyses and screens based on fully automated image cytometry (for cell-by-cell and sub-cellular compartment measurements) create a vast wealth of information in a hands free, unbiased manner[1-4].

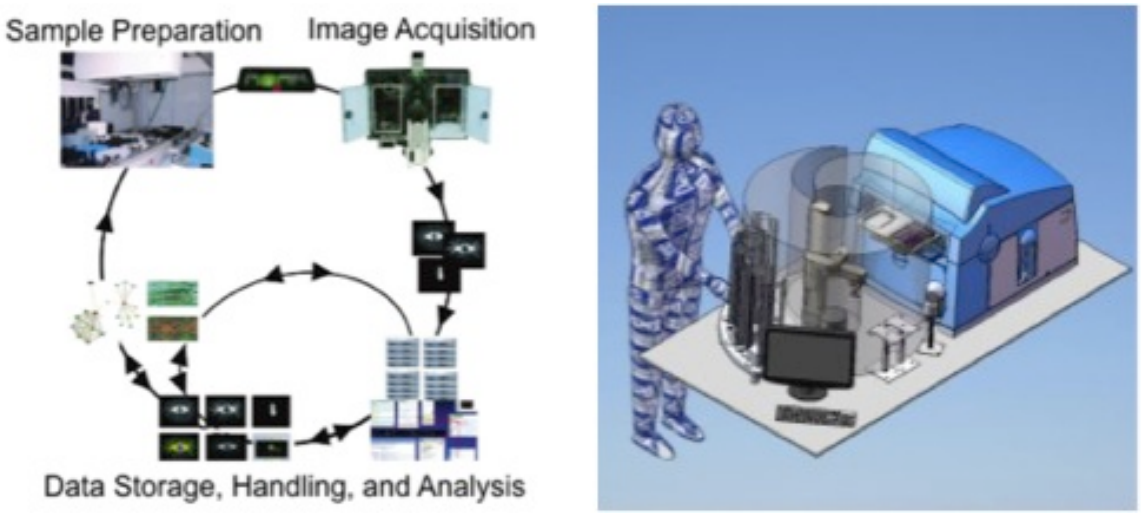

Figure 1.1: The principles of High Content Screening. Automated handling to provided stand-alone performance.

As a basic definition, HCS can be described as a multi-tiered approach to acquire and analyze large volumes of biologically relevant data captured from traditional and novel inverted light microscopy (confocal, epi-fluorescent, reflective, transmitted, etc). Image based HCS combines modern cell biology,

automated microscopy, and robotic handling to produce spatially or temporally resolved datasets that contain important phenotypic and morphological parameters in the cellular systems under investigation. Image based HCS assays are performed in 96-, 384-, and 1536- well microtiter plates (MTP) and typical assays measure drug effects, cytotoxicity, apoptosis, cell proliferation, and nucleocytoplasmic transport. This technology is used heavily in the pharmaceutical industry for drug discovery and as a general tool in academic research for large-scale cellular biology.

1.2 Background & Significance

Using fluorescence and epi-fluorescence based imaging modalities, HCS allows researchers to simultaneously capture multiple measurements from individual cells including cellular morphology, cell-cycle dynamics, molecular co-localization, metabolic state, motility, and texture in fixed and live-cell imaging environments. The downside to image based HCS, when compared to other techniques, is the speed of data acquisition. Image based HCS quality/performance (e.g., precision, accuracy and dynamic range of measurements) is directly linked to the contrast and resolution (detail) available in each image, and is thus dependent on the quality of focus when the data is acquired. If the specimen being screened is not in focus (residing at the best focal plane based on the optical setup) or if the integration times used during acquisition are too high or too low, the information gathered is erroneous and no significant statistical or experimental claims can be made.

1.3 Autofocus

Due to HCS being predominately computer controlled and largely user independent, guaranteeing image data captured reside at the best focal plane is largely dependent on the surface topology of the optically clear membrane of the MTP (glass, polystyrene, polyethylene or other polymer) if reflective positioning is used and / or image based focus routines if using a through focus stack.

Autofocus routines are used to help ensure that “best-focus” is maintained during data acquisition. Autofocus can be carried out either by reflective

positioning or by direct sharpness measurements of a through-focus image stack. Depending on hardware setup autofocus routines can run from milliseconds to seconds.

“Best focus” is defined as the optimal focal plane in which the specimen has the highest sharpness. A more quantitative definition defines the best focus position as the focal plane with the largest mid to high spatial frequencies.

Autofocus is the crux of any automated system because it ensures the images acquired during the scan are not subject to out-of-focus blur. This is especially important when using high numerical aperture (NA) objectives (>0.5). As the NA of the objective increases, the light collection ability increases, the resolving power of the system increases, and the depth of field (depth of focus) decreases. HCS screens primarily use epi-fluorescence illumination. This imaging modality enables targeted illumination of the specimen by labeling various regions of interest with fluophores (fluorescent dyes, proteins, or quantum dots), using a dedicated light (arc-lamp, laser line, etc.) and the correct excitation/emission filters. Low concentrations of the fluorescent agents are used to prevent/reduce phototoxic effects that could alter the state of what is being visualized. Because of this, high NA objectives are essential, along with very high quantum efficiency detectors, to enable optimal specimen interrogation.

Focus routines that use reflective positioning keep the objective of the microscope a certain distance from the bottom surface of the MTP or glass cover slip of a microscope slide at all times. This will allow the specimen of interest to

remain in a pre-determined focus position relative to the optical axis. This focus position, and relative displacement distance from the objective is determined with an image based focus routine or is set via human interaction. Monitoring the surface contours of the MTP and dynamically adjusting the Z-Axis position of the microscope objective maintain the displacement distance. The objective is typically moved using a piezo stage or Z-stepper motor. This technique is scene independent because there is no analysis of image content. This technique is also very rapid because no image acquisition or post-capture processing is required. It however, is dependent on the ability to properly track surface topology and correlate said measurement with the best focus position of the target specimen[6-8].

Autofocus routines dependent on scene content on the other hand rely on: proper image acquisition (i.e. no photo-bleaching or image saturation); content within the image (a blank field can lead to improper focus determination); mechanical stability of the microscope focusing column or Z-Focus piezo unit to ensure proper sampling of a through focus stack; and the correct focus analysis (proper extraction of pertinent features related to focus). Previous graduate students in the Jeff Price lab have developed standards that help guide best focus determination when using image based autofocus routines[9-13].

Autofocus routines, multi-stage fluorescence capture (depending on the number of fluorescent channels used), and stop and go stage motion to position

the automated stage for each data point captured all contribute to the slow performance of image based HCS systems.

1.4 The Z-Prime Score and HCS Data Analysis

A Z-prime score is a metric used to determine the value of performing a High Content Screen. Because of the costs and prep time associated with large screens, a metric that can quickly determine the validity of performing the desired screen is essential. The Z-prime score looks at the difference between the positive and negative control population for a given experiment. In HCS, because there are many features available, a Z-prime score can, and typically is, generated for each feature measured. The z-prime score uses the mean and standard deviation of the positive and negative controls in a simple distance formula and reports how close or far a part the two are. A Z-prime score ≥ 0.5 is generally considered to be the threshold required to make a screen worth doing.

$$Z - Prime = 1 - \frac{3(\sigma_p + \sigma_{n)}}{|\mu_p - \mu_n|}$$

The Z-Prime Score rates the validity of performing a large-scale screen, and also functions as a simple way to process large volumes of image data (gigabytes to terabytes). HCS datasets are intended to be rich with features and having a method to condense the image data into metrics that can be quickly parsed, sorted and ranked proves an invaluable tool in understanding the outcome of complex biological processes in robust objective and systematic way.

Image processing techniques use de-convolution, Fourier analysis, linear algebra, and other various algorithms to segment image data for the identification of cells, nuclei, and cellular microstructures (organelles, mitochondria, etc.). These techniques rely on quality and clarity of fluorescence labels, oblique or dark-field illumination, and other microscopy techniques to properly record the biological scene being recorded while HCS scans are being performed. Morphological and phenotype features of biological systems can be recorded, evaluated and scored. This feature analysis is however useless if the image encoded the information is out of focus or blurred. HCS image processing and the Z-Prime score are directly affected by the quality of focus. Thus the necessity to use cumbersome focus routines to guarantee a best “in-focus” image is captured for each data point in an HCS screen.

1.5 High Content Screening Technology

Current medium magnification (10x to 40x), high-resolution (≥0. 5NA) image based HCS instruments employ screening rates of approximately 20,000 to 50,000 wells per day. This allows for roughly 1.73 to 4.32 seconds per well for interrogation time, 1 to 4 image(s) per well, and translates to thousands of cells scanned per second depending on objective magnification, camera pixel size, and cell diameter[4].

Examples of commercially available systems include Beckman Coulter IC 100, GE Amersham InCell 1000 and InCell 3000, MAIA Scientific Mias-2, Cellomics ArrayScan, Perkin Elmer Opera, and Aperio ScanScope.

Table 1.1: Chart comparing HCS instruments in terms of resolution, data capture time, and well throughput

	Low Magnification	Medium Magnification	High Magnification
Useful resolution:	~500 μm	~20 μm	~1 μm
Typical Target Size:	1 mm–1cm	50–250 μm	0.5–50 μm
Imaging time/plate:	Milliseconds to minutes	Minutes	Minutes to tens of minutes
Throughput wells/ day:	Up to hundreds of thousands	Tens of thousands	Thousands to tens of thousands
Examples:	GEH LEADSeeker, PELS Viewlux	PELS FMAT, TTP LabTech Acumen Explorer	GEH IN Cell 1000/3000, Perkin Elmer Opera, Molecular Devices ImageXpress, Beckman Coulter IC 100

These systems usually employ raster scanning to traverse each row going well to well in a stop and go fashion and goes to each field of view (FOV) per well in a similar fashion.

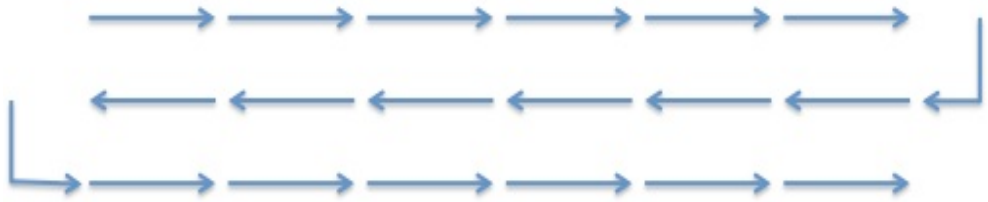

Figure 1.2: Graphic describing the snake-like pattern followed during a typical HCS scan.

Scanning time includes the following:

- Auto-focus time to ensure the sample, which is uneven due to both the substrate and the tissue on top of the substrate (see Fig. 1.3), is in best focus by adjusting either a piezo stage or objective fine focus position:
    - Direct sharpness measurements of a through-focus image stack (slow, provides best focus based on well content)
    - Reflective positioning (fast, maintains relative distance between objective and MTP membrane surface)
- Charge Coupled Device (CCD) or Photo-Multiplier Tube (PMT) exposure time
- Arc Lamp or Laser Shutter times, if fluorescence is used
- Acceleration times to go from rest to cruising velocity and back to rest
- Cruising velocity times while moving between fields

- And if multiple fluorescence channels are being screened:
    - Time required to swap excitation/emission filters
    - Additional auto-focus time, if needed
- Repeat sample collection time

These steps in the data collection train, although required to maintain the high fidelity of image based HCS performance, cause slow screening times when repeated for each image acquired in the varied MTP formats and thus hinder its attraction to experimental studies requiring truly high-throughput screening times.

As an example, large-scale screens of tens of thousands to millions of compounds and potential clinical diagnostic applications (e.g., rare cancer cell detection in blood) would benefit from increased image acquisition speeds. Microtiter well plates used in HCS, allow for multiple experiments to be performed simultaneously. Increasing the number of wells scanned in a day equates to increasing the number of different experiments performed.

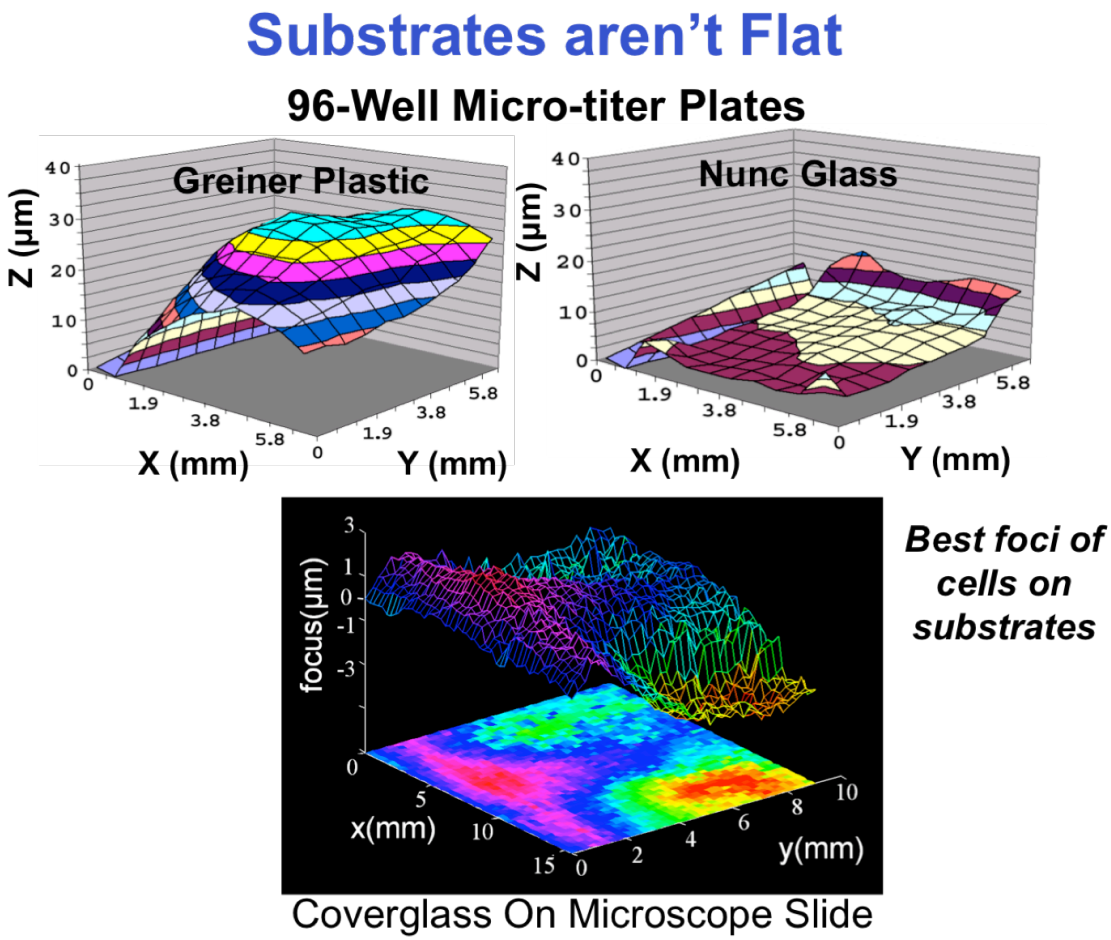

Figure 1.3: Graphs show topology mapping of well plate bottoms and cover glass surfaces. Well plate membrane bottoms can be composed of glass or any number of various films (cyclo-olefin polymer, polyethylene, polypropylene, polystyrene). These substrates, when fused/mated to the well plate by either adhesive or heat treatment, tend to bend/warp and settle with a heterogeneous surface profile (can vary by as much as 200 μm to 300 μm). Bravo et al, 2001[11].

The goal of my thesis, the development of a continuous high content screening scanning system, is to expand the bandwidth of data collection for fixed end-point screening assays by developing a high content screening platform capable of scanning over 100,000 wells per day (approximately 260 SBS standard 384 well microtiter plates) at 10x magnification or 50,000 wells per day (approximately 130 SBS standard 384 well microtiter plates) at 20x

magnification. The system will capture 3 fluorescent channels (Red, Green and Blue) simultaneously while maintaining image focus using a combination of reflective positioning (laser based focus) and image-based focus. The system will also capture every available field of view going across an individual well from left to right (6 to 10 frames depending of magnification).

Unfortunately microtiter well plates, especially those with plastic membranes (polystyrene, poly-ethylene, etc.) as their bottoms, are notorious for not being “flat” and have uneven surface profiles. This means that each well has a different optimal “best focus” plane. Moreover, each field of view in each well might also have a different “best focus” plane. This variance in surface topology removes the ability to simply increase the scan speed of a well plate without regard to “best focus.” Doing so would result in simply acquiring a lot of out of focus useless data.

As consequence, going from the current upper screening rate threshold to the high-throughput regime (scanning greater than 100,000 wells per day) isn’t simply a matter of increasing the number of plates scanned in a given day with current techniques. The limitations of stop and go motion, the necessity for each image acquired to be in focus, and multi-channel capture require new timing strategies to be implemented in order to increase the bandwidth of high resolution image based HCS.

1.6 History of Time Delay and Integration Imaging

Time Delay and Integration Imaging (TDI) is a method for blur-free capture of moving images was created in 1973 at Sarnoff[5]. This technique preserves sensitivity and image quality even with fast relative movement between the detector and the objects being imaged.

As with any CCD, image photons are converted to photocharges in an array of pixels. During TDI operation the photocharges are continuously shifted from pixel to pixel down the detector, parallel to the axis of flow. By synchronizing the photocharge shift rate with the velocity of the flowing cell, the effect is similar to physically panning a camera[6].

The Price Lab has a long history of demonstrating the ability to use TDI and enable volume imaging as well as early proof of rapid HCS[6-12]. In addition, various groups have demonstrated the potential of combining TDI with traditional Image Cytometry to create a rapid HCS platform for detecting CTCs, rare cells, and for monitoring flow. Studies correlating noise and performance characteristics of TDI CCD imaging relative to traditional CCD techniques has enabled use of this versatile image capture technique as a means to acquire blur free images of moving scenes while maintaining high SNR and long integration times[13-18].

1.6 The Problem

As aforementioned, the downside to image based HCS, when compared to other techniques, is the speed of data acquisition. Image based HCS quality /

performance (e.g., precision, accuracy and dynamic range of measurements) is directly linked to the contrast and resolution (detail) available in each image, and is thus dependent on the quality of focus when the data is acquired. As consequence, going from the current upper screening rate threshold to the high-throughput regime (scanning greater than 100,000 wells per day) isn't simply a matter of increasing the number of plates scanned in a given day with current techniques. The limitations of stop and go motion, the necessity for each image acquired to be in focus, and multi-channel capture require new timing strategies to be implemented in order to increase the bandwidth of high resolution image based HCS.

To address these issues, a new strategy is required in terms of data collection that will allow continuous acquisition of data at rates sufficient to bring HCS into the high throughput regime.

In an effort to help in this cause, my research focused on bringing together existing imaging, data capture motifs, and novel microscopy techniques to allow for a continuous scanning system capable of acquiring in focus, statistically relevant high content image data. The research was broken into three sections. The sections involved system design and hardware setup, software development, and finally system testing and validation.

1.7 The Goal

The goal of the continuous HCS system is to expand the bandwidth of data collection for fixed end-point screening assays by developing a high content

screening platform capable of scanning over 100,000 wells per day (approximately 260 SBS standard 384 well microtiter plates) at 10x magnification or 50,000 wells per day (approximately 130 SBS standard 384 well microtiter plates) at 20x magnification. The system will capture 3 fluorescent channels (Red, Green and Blue) simultaneously while maintaining image focus using a combination of reflective positioning (laser based focus) and image-based focus. The system will also capture every available field of view going across an individual well from left to right (6 to 10 frames depending of magnification).

This was implemented using materials and methods described in the following sections:

System Design and Hardware Setup (Chapter 2)

Develop HT-HCS platform for scanning more than 100,000 wells per day in 384- well microtiter plates at 10x and 50,000 wells per day 20x magnification using medium to high-resolution optics (≥ 0.5 NA).

Software Development - Hardware Control (Chapter 3)

Develop Software Control and Incorporate Robotics to Control System for stand-alone operation.

System Testing and Validation (Chapter 4)

Characterize System Performance Qualitatively and Quantitatively using control assay and biological assays being screened at the Sanford-Burnham Center for Chemical Genomics.

Chapter 2: *System Design and Hardware Setup*

***Section Overview*:** Develop HT-HCS platform for scanning more than 100,000 wells per day in 384- well microtiter plates at 10x and 50,000 wells per day 20x magnification using medium to high-resolution optics (≥ 0.5 NA)

2.1 Hardware Description

- ***Microscope, Camera, Light Source, Motorized XY Stage, Piezo Z-Focus Stage, Robotics***

A combination of commercially available equipment and engineering design to convert a normal automated microscope into a HT-HCS platform capable of scanning > 100,000 microtiter wells in a 24 hour period was employed. The hardware is: a fully automated Nikon TE2000-E inverted microscope, an automated BioPrecision2 extended travel XY-Stage from Ludl, an optical linear encoder from Micro-E (the Mercury II 5800), a customized Hamamatsu 3-CCD C7780-50 camera equipped with Time Delay and Integrate (TDI) functionality, an off-the-shelf Keyence laser displacement sensor capable of tracking displacements within 2 mm (LK-G15), a Physik Instrumente (PI) 500 μm Piezo Z-Stage, and a Lumencor Aura light engine fluorescent light source.

Combined and controlled using custom software, the system hereafter referred to as “the TDI Continuous Scanning System (TDI-CS System)” is capable of using dynamic laser based autofocus to maintain “best focus” while data is being acquired at almost video rate (≅6 to 9 frames per second). This translates 6 to 10 images per well in 384- well MTP being scanned depending on

objective magnification (10x or 20x) for a total image count of 1,920 to 3,840 images per plate in less than 30 minutes. For 1536- well microtiter plates this becomes 3 to 6 images per well being scanned for a total of 4,608 to 9,216

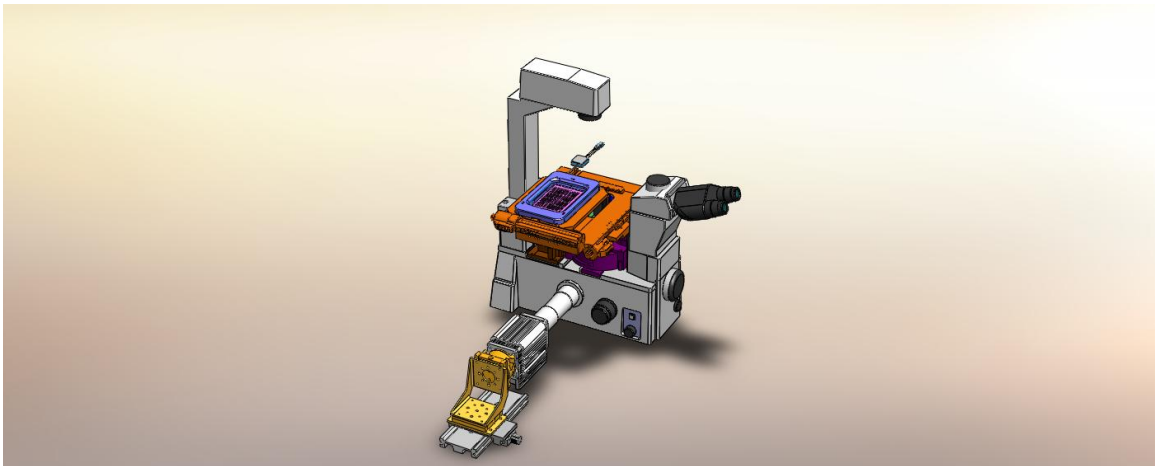

Figure 2.1: Schematic Depicting TDI Continuous Scanning System

images per plate in under 60 minutes.

The three main components of the TDI-CS System are the:

Microscopy Component:

- Nikon TE-2000-E fully automated microscope
- Lumencor Aura Light engine - 3 color adjustable fluorescent light source

The automated microscope allows for the dynamic switching of objectives, filters, condenser annulus rings, optical light path, and objective focus position on-demand. The lumencor light engine allows for the customized setting of individual excitation wavelength intensity for Red, Green and Blue channels. This

allows for the normalization of exposure time across a wide spectrum of fluophores.

Continuous Imaging Component:

- Hamamatsu 3CCD C7780-51 TDI camera
- Ludl Bioprecision2 XY Stage
- Micro-E Linear Encoder - Mercury II 5800

Time Delay and Integrate (TDI) is a CCD technique that allows for the imaging of moving objects and is especially suited for low light scenarios. This is accomplished by synchronizing the vertical line rate (measured in Hz or pixels / sec) of the CCD camera to the velocity of the moving object. The vertical line rate of a CCD camera describes how long it takes for one vertical line to be clocked downward to the next transferring the accumulated charge of each pixel within the vertical line with each step. This allows for the exposure time to become a function of vertical line count and not how long the camera's shutter is open. This is a very useful technique in live cell imaging to prevent photo-toxicity. As long as the vertical line rate is matched with the velocity of the moving target within 1% to 4%, the moving scene is effectively captured in without linear motion blur.

The TDI vertical line rate is triggered by a TTL level signal delivered by the Micro-E Mercury II 5800 linear encoder attached to the X-Axis of the Ludl XY microscope stage. Using a Divide-By-N timing circuit, the linear encoder signal

from the horizontal axis (long direction) of the Bioprecision2 stage is decimated to create the corresponding frequency required to synchronize the TDI camera line rate to the stages velocity.

The relationship between Vertical Line Rate and Object Velocity is:

- Velocity (µm/s) = Effective Pixel Size (µm/pixel) x Line Rate (pixel/s)
- Effective Pixel Size: Camera Cell Size (µm/pixel) / Optical Magnification

With the ability to image a moving object, the stop and go motion currently present with current HCS systems can be completely removed and can be replaced with a control scheme that allows for continuous data capture almost 100% of the time. Acceleration of the stage through the empty wall regions of the MTP can help reduce the capture of erroneous information and speed up plate scan time, if desired[14-16].

Using a 3-CCD chip camera, the C7780-51, (true RGB) also allows for the simultaneous acquisition of up to three fluorescence channels. The camera also has individual channel gain control. When operating in TDI mode, each of the chips exposure times are equal. This is not particularly desirable when imaging fluorophores that require different exposure times. DAPI, FITC and TX-Red are three commonly used fluorescent proteins. DAPI usually requires around 10 ms to 75 ms of exposure. FITC and TX-Red require from 100 ms to 1000 ms of exposure depending on concentrations used. In TDI mode this equates to either

over exposing the DAPI channel if the line rate is matched to the FITC or TX-Red exposure requirement or underexposing FITC and TX-Red if the vertical line rate is matched to DAPI's exposure requirement[17-18].

Using a combination of bandpass filter cubes (Semrock), individual channel gain settings, and the Lumencor Aura light engine to set different excitation intensitie s proper illumination of fluorophores without causing photo-bleaching or pixel saturation is achieved. This helps resolve the aforementioned problem of exposure time misalignment across the different channels when driving the camera at a specific vertical line rate. This does not however, remove fluorophore emission bleed-through common when doing simultaneous multi-channel capture.

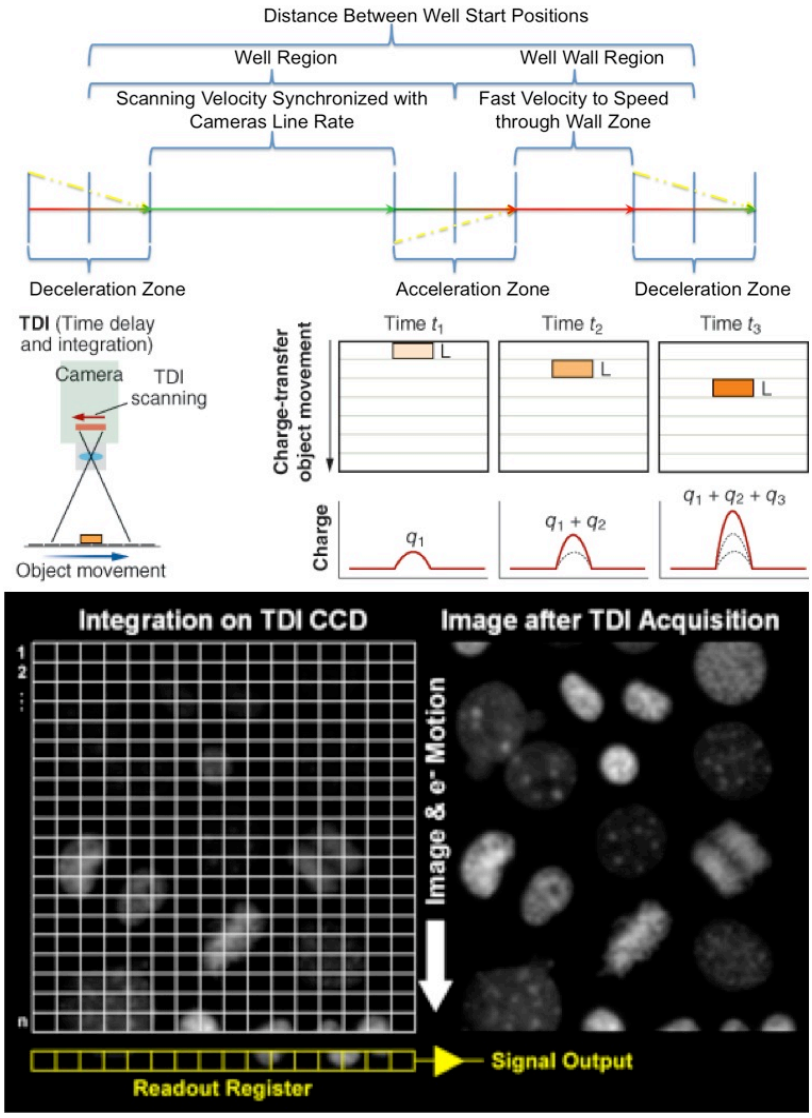

Figure 2.2: (a). Schematic showing velocity and acceleration profile of travel through well. (b). Time delay and integrate (TDI) is a method of scanning moving objects. As the CCD moves from one vertical line of pixels to the next, the integrated charge moves along with it, providing higher resolution at lower light levels than with a line-scan camera. (c). Schematic showing cells as they are scanned using TDI Image Acquisition.

Dynamic Autofocus Component:

- PI 500μm Piezo Stage
- Keyence Laser Displacement Sensor

Reflective Positioning for autofocus is a well-established technique proven to work well when imaging glass slides and to some degree, microtiter well plates. Ultrasonic or laser based positioning systems can be used for reflective positioning. The technique usually involves triangulating the distance between the laser source, the reflecting surface, and the incident reflection on a CCD chip or quad detector. The path length between the laser head and the reflecting surface is calculated using the Law of Sines. Reflective positioning systems can also measure the relative diameter of a projected image reflecting back from a laser surface. With this technique the relative laser focal spot size is correlated to best focus position. Each technique requires a calibration of the best focus position prior to use. The pre-calibration can be a manual setting of the microscope objective in best focus position or can be done using image based autofocus.

Commercial systems like Nikon's Perfect Focus Automated microscope and Olympus Scan^R automated microscope use reflective positioning as their means for maintaining best focus when scanning glass slides and MTPs.

- The Nikon PFS uses a through the objective implementation of reflective positioning.

- Olympus Scan^R uses the triangulation method described above and places the laser sensor into one of the available slots in the objective turret.

Using reflective positioning and a fast large travel range piezo stage allows for the dynamic repositioning of the MTP to ensure the “best focus” plane is captured while scanning in Continuous Motion TDI mode.

2.2 Hardware Specifications

Automated Inverted Microscope. The Nikon TE2000-E is an inverted epi-fluorescent microscope with nanoprecision Z-axis control. The microscope uses Nikon's CFI60 infinity optical system, and has a parfocal distance of 60 mm. The microscope has a revolving nosepiece that can hold up to 6 objectives; Intermediate magnification selectable from 1x-1.5x; We added a continuous video zoom lens (0.95x-2.25x) in order ensure that we matched the effective pixel size of the camera with the stages TTL signal. Contains 5 light path positions and a motorized position changer: Observation: other ports: 0/100 (fixed); Left port: 100/0 (fixed); Right port: 20/80 (fixed); Front port: 20/80 (fixed); Bottom port: 0/100 (standard).

Z-Focusing via motorized/manual nosepiece up/down movement; Stroke from standard position: manual up 7 mm, down 3 mm, motorized up 6 mm, down 2.5 mm; Coarse stroke: 4.9 mm/rotation; Fine stroke: 0.1 mm/rotation (motorized); Minimum fine reading: 0.05 μm (motorized control from remote control pad; optical linear encode incorporated); Refocusing stopper; Adjustable coarse torque stopper.

Epi-Fluorescence light capabilities with a motorized filter cube cassette that sits below the objective nosepiece. The cassette holds up to 6 filter cubes (a block containing the excitation, emission and dichroic mirror to enable epi-fluorescence image capture).

Fluorescent Light Source. We added a Lumencor Aura Light Engine to the system. The Aura Light Engine is an alternative epi-fluorescent light source solution when compared to traditional mercury arc lamp or dedicated laser-line source. The unit comes with three dedicated excitation wavelengths (UV, Cyan, Green) that can be controlled independently via rs-232 communication or digital I/O.

Automated XY-Stage. The microscope is outfitted with an automated BioPrecision2 extended travel XY-Stage from Ludl. The BioPrecision2 stage is a stepper motor driven stage capable of traveling 170 mm in the X-direction and 100 mm in the Y-direction. The unit has a 2mm pitch lead-screw and a 50nm resolution optical encoder on both X and Y axes. The unit is controlled using National Instruments motion control hardware suite (MID-7604 power drive and PCI-7350 stepper motor controller) and NI-Motion software. The MID-7604 is a 4-axis stepper motor power amplifier with a wide range of stepper motor micro-stepping capabilities as well as configurable current limit settings. For the BioPrecision2, the MID-7604 is set to 250 microsteps per step and has 1 amp peak current output. 250 microsteps per step translates to 50,000 steps per revolution of the 1.8° shaft or 25,000 steps per millimeter.

Precision Linear Encoder. We added to the X-Axis of the Ludl stage a compact high resolution Micro-E 5800 series linear encoder capable of reaching resolutions down to 1.2nm. The Micro-E encoder is an optical encoder that

provides a quadrature TTL (Transistor Transitor Logic) signal based on the gratings of a glass or plastic scale. Quadrature encoders provide both displacement and directional information by outputting two signals (A and B). The

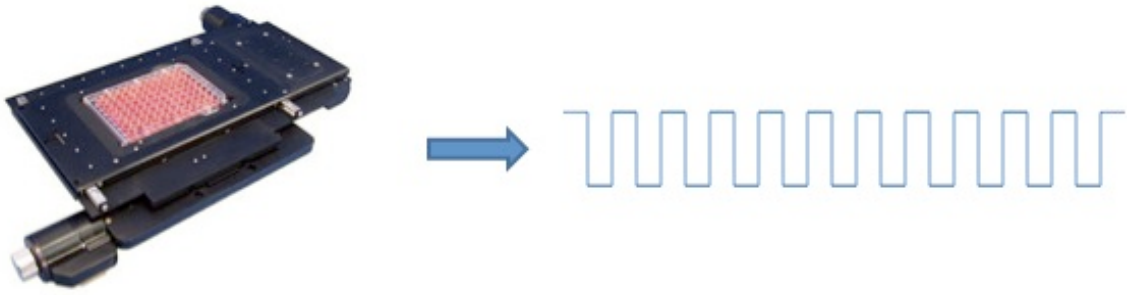

Figure 2.3: Schematic showing the Ludl Bioprecision2 XY microscope stage and a corresponding TTL level signal generated as the stage moves. This TTL pulse is used to synchronize the vertical line rate of the C7780-51 TDI camera and the stages horizontal travel velocity.

signals are 90 degrees out of phase with respect to each other. The native pitch of the grating is 20 microns and can be interpolated down (by up to 16384) to provide nanometer resolution. We have an interpolation factor of 8000 to give us an encoder resolution of 2.5 nm (20 microns / 8000). When coupled to the X-axis of the Ludl BioPrecision2 stage, this translates to 800,000 encoder counts per revolution or 400,000 encoder counts per millimeter.

Divide-By-N Counter. We introduced a divide-by-n counter to convert the native TTL signal from the linear encoder mounted to the X-Axis of our Ludl stage to the desired line-rate of the CCD camera. To do this, we use a Motorola MC14018B Divide-By-N counter IC. A divide-by-n counter is essentially a frequency divider based on a preset divisor. For every N-pulses that are fed into

the counter, once the divisor count is reached one TTL level pulse is output. With our encoder resolution of 2.5 nm, depending on magnification (10x or 20x) and intermediate zoom (1.075x), a division by 60 or 30 is required to have the TTL pulse train match the effective pixel size of the camera (0.6 microns/pixel or 0.3 microns/pixel). Using frequency division by 60 or 30 allows for the 2.5 nm resolution of the encoder to be transformed to the desired 600 nm or 300 nm per pulse respectively.

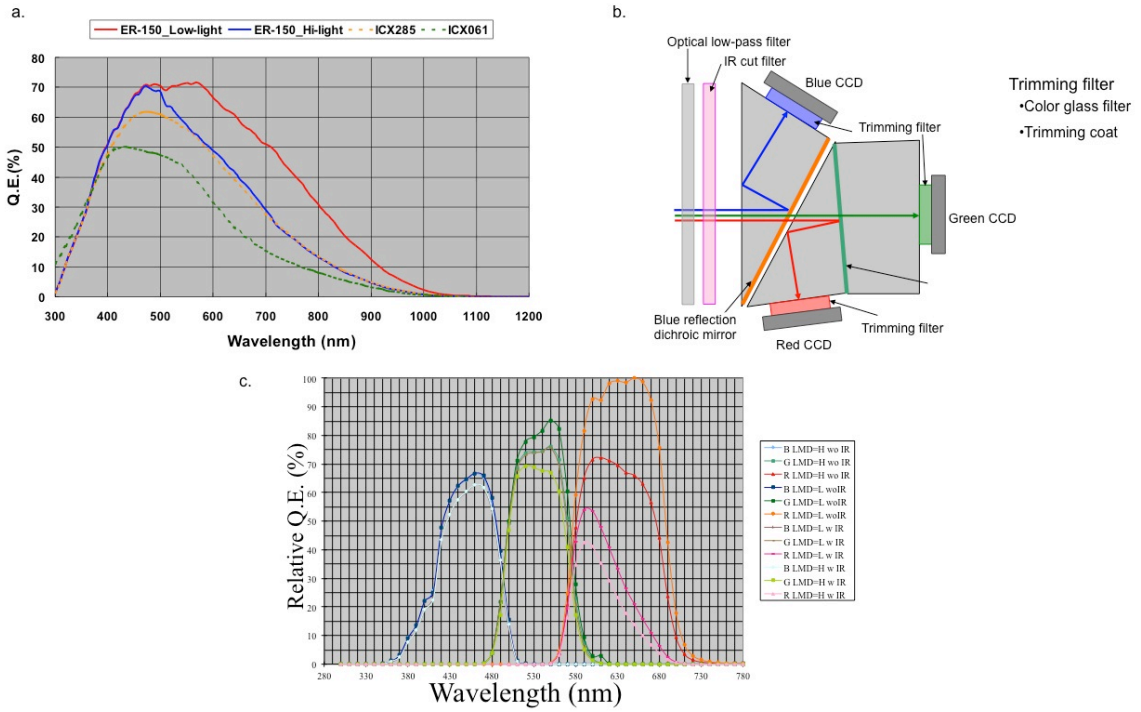

Figure 2.4: (a). Graph showing quantum efficiency of the Sony ER-150 CCD chip used by the C7780-51 TDI camera. (b). Schematic showing the layout of the 3-CCD chips contained within the C7780-51. (c). Graph showing the relative quantum efficiencies of the 3-CCD chips as well as the spectral overlap of each CCD.

CCD Camera. We use a multi-channel 3CCD (charge coupled device) Hamamatsu Camera, the C7780-51. The camera is capable of capturing images using Time Delay and Integrate Capture, with a maximum line rate of 8 kHz. The camera performs unidirectional TDI. The camera has 1344 horizontal pixels and 1024 vertical pixels, a bit-depth of 12 expanded into 16 bits (data range is 0 to 4095), and 3 channels per pixel. This translates to each captured frame having a storage size of 8.257 megabytes (MB). The pixel cell size is 6.45 µm x 6.45 µm. The camera has independent channel gain control and varies 1x, 2.5x, and 5x.

To set the independent channel gain, one must first set the max gain, 1-5x, and then set a percentage of the max for each channel (0-100%).

Reflective Position Sensor. We use a Keyence LK-G15 laser based reflective position sensor to perform our surface topology measurements. The LK-G15 displacement sensor uses triangulation (Law of Sines) to map optical displacement to a position. The unit is capable of rapid position sensing and has a measurement range of +/- 1 mm (2 mm total), a reference standoff of 10 mm, a spot size of 20 µm x 500 µm, and a resolution of 10 nm. The sensor is capable of tracking up to 4 internal reflections (index of refraction changes within a material). This allows us to profile either the top or bottom surface of a MTP membrane or glass cover slide.

Long Travel Piezo Stage. We use a Physik Instrumente (PI) piezo driven Z-axis stage to perform rapid 2D image based autofocus as well as dynamic autofocus in conjunction with our reflective position sensor. The stage is able to travel up to 500 microns and is controlled using analog voltage +/- 10 V coming from a National instruments data acquisition I/O board (PCI-E -6251).

Microtiter Well Plate (MTP). Society for Biomolecular Sciences (SBS) standard 96, 384, and 1536 well microtiter plates all take up the same dimensions 127.76 mm x 85.48 mm. A 96 well dish has typical well size of 6.39mm x 6.39mm. A 384 well dish has typical well size of 3.3mm x 3.3mm. A 1536 well dish has typical well size of 1.53mm x 1.53mm.

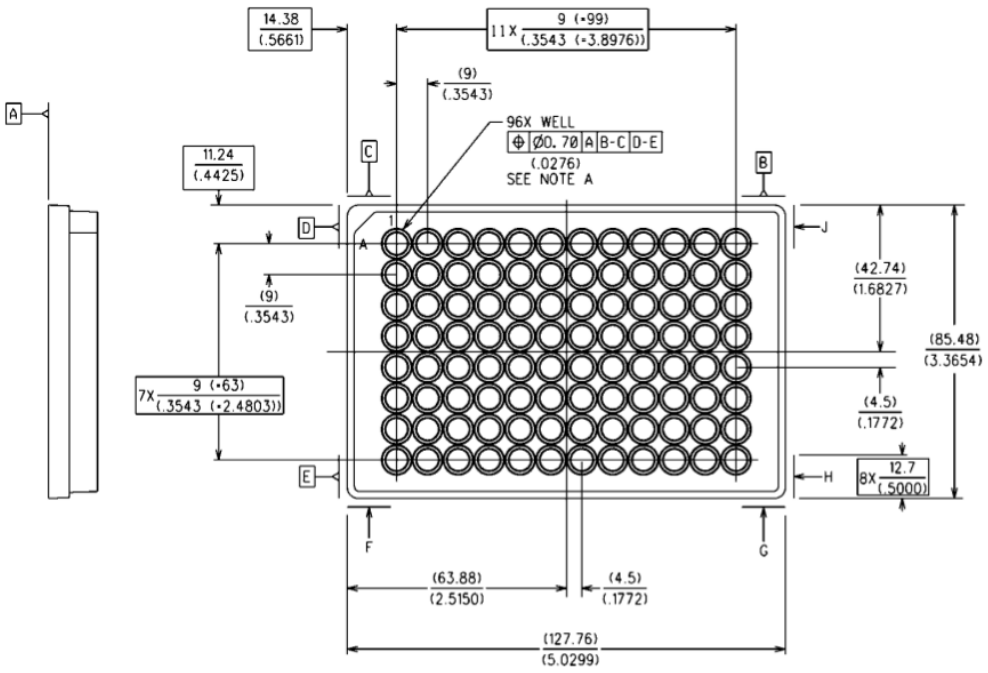

NOTES:

1 The drawing standard used is ASME Y14.5M-1994

2 The geometry shown is for illustration only and does not imply any preferred or required construction.

3 Dimensions shown are: Millimeters / (Inches)

4 Dimensions and tolerances do not include draft.

A The top left well of the plate shall be clearly marked (e.g.: on the left with the letter "A" or the numeral "1", or at the top with the numeral "1"). Additional markings may be provided.

Figure 2.5: Schematic showing the layout and dimensions of an SBS standard 96 well microtiter plate

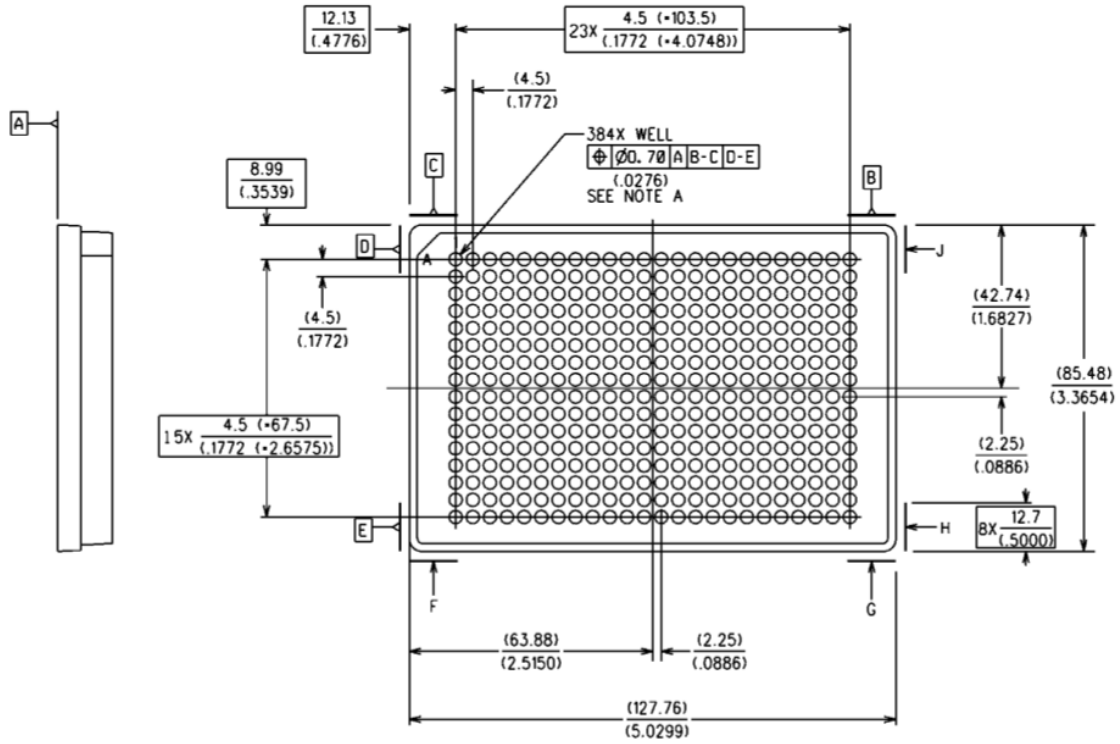

NOTES:

1 The drawing standard used is ASME Y14.5M-1994

2 The geometry shown is for illustration only and does not imply any preferred or required construction.

3 Dimensions shown are: Millimeters / (Inches)

4 Dimensions and tolerances do not include draft.

A The top left well of the plate shall be clearly marked (e.g.: on the left with the letter "A" or the numeral "1", or at the top with the numeral "1"). Additional markings may be provided.

Figure 2.6: Schematic showing the layout and dimensions of an SBS standard 384 well microtiter plate

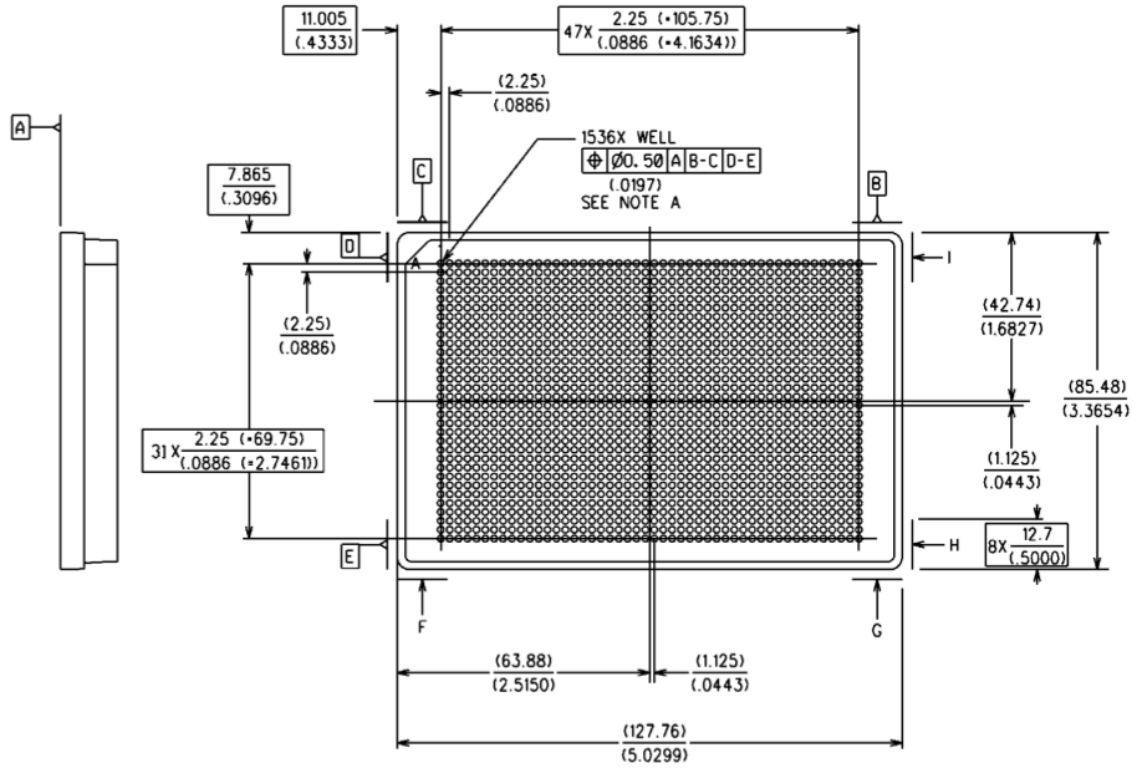

NOTES:

1 The drawing standard used is ASME Y14.5M-1994

2 The geometry shown is for illustration only and does not imply any preferred or required construction.

3 Dimensions shown are: Millimeters / (Inches)

4 Dimensions and tolerances do not include draft.

A The top left well of the plate shall be clearly marked (e.g.: on the left with the letter "A" or the numeral "1", or at the top with the numeral "1"). Additional markings may be provided.

Figure 2.7: Schematic showing the layout and dimensions of an SBS standard 1536 well microtiter plate

2.3 TDI Performance

Given the nature of Time Delay and Integrate imaging, the camera's line rate dictates the maximum performance (speed) of any TDI based imaging application. If there is a mismatch in target velocity versus the camera's line rate, the captured images will have considerable motion artifact (blur). Motion blur, if present, comes in the form of streaks and smearing of pixel information in the direction of motion. To help avoid motion blur, we determined the maximum performance conditions in which the TDI Continuous Scanning System would operate. Using the aforementioned equations for effective CCD pixel size and stage velocity as a function of camera line rate, we found that the maximum stage velocity is 4.8 mm/s using the camera's max line rate (8 kHz), 10x objective magnification, camera pixel size (6.45 µm x 6.45 µm), and an intermediate camera zoom of 1.075x.

- Velocity (µm/s) = 4,800 (µm/s) = 0.6 (µm/pixel) x 8000 (pixel/s)
- Effective Pixel Size: 0.6 (µm/pixel) = 6.45 (µm/pixel) / (10 x 1.075)

Table 2.1: The following chart gives example stage velocities as function of desired line rate and magnification:

Line Rate (pixel/s)	Objective Magnification	Intermediate Zoom	Pixel Size (µm/pixel)	Effective Pixel Size (µm/pixel)	Divide By N	Linear Encoder TTL (Hz)	Stage Velocity (µm/s)
1,000	10x	1.075x	6.45	.6	60	60,000	600
	20x			.3	30	30,000	300
2,000	10x	1.075x	6.45	.6	60	120,000	1200
	20x			.3	30	60,000	600
3,000	10x	1.075x	6.45	.6	60	180,000	1800
	20x			.3	30	90,000	900
4,000	10x	1.075x	6.45	.6	60	240,000	2400
	20x			.3	30	120,000	1200
5,000	10x	1.075x	6.45	.6	60	300,000	3000
	20x			.3	30	150,000	1500
6,000	10x	1.075x	6.45	.6	60	360,000	3600
	20x			.3	30	180,000	1800
7,000	10x	1.075x	6.45	.6	60	420,000	4200
	20x			.3	30	210,000	2100
8,000	10x	1.075x	6.45	.6	60	480,000	4800
	20x			.3	30	240,000	2400

In traditional HCS screening, image capture follows a raster scan snake-like pattern, where the stage moves from well to well in each row from left to right and then wraps around to the next row and moves from right to left… etc.

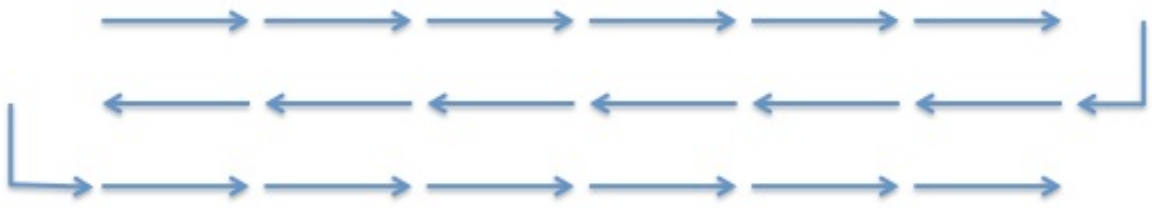

For SBS standard plates, the active imaging area is typically an inner bounding rectangle of 106 mm x 75 mm regardless of well count. A 96-well dish has 8 rows, A-H, and 12 columns. A 384-well dish has 16 rows, A-P, and 24 columns. A 1536-well dish has 32 rows and 48 columns. Using a traditional snake-like pattern to scan the active imaging area requires stop and go positioning in each available well. Due to this, the scan time required for imaging a 96-, 384-, or 1536- well dish is dependent on the number of wells per row and the number of rows per plate. However, for a continuous scanning system the number of wells per row is not important and only the physical length of the row and number of rows per plate determine the scan time. SBS standard plates are all equivalent in row length and thus only the number of rows per plate differentiates the scan time per plate type (96, 384, and 1536). From the above chart we see that using a 20x objective, 1.075x intermediate camera zoom, and line rate of 8,000 Hz gives us a stage speed of 2400 µm/s or 2.4 mm/s. With that velocity, the time required to scan each row (106 mm) is approximately 44.2 seconds (time = distance / velocity).

Table 2.2: The time required to scan an entire plate is as follows:

Line Rate (pixel/s)	Stage Velocity (mm/s)	Distance (mm)	Time to Scan Single Row (s)	Plate Time (min) (96 Well @ 8 Rows)	Plate Time (min) (384 Well @ 16 Rows)	Plate Time (min) (1536 Well @ 32 Rows)
1,000	0.600	106	176.7	23.6	47.1	94.2
	0.300		353.3	47.1	94.2	188.4
2,000	1.200	106	88.3	11.8	23.6	47.1
	0.600		176.7	23.6	47.1	94.2
3,000	1.800	106	58.9	7.9	15.7	31.4
	0.900		117.8	15.7	31.4	62.8
4,000	2.400	106	44.2	5.9	11.8	23.6
	1.200		88.3	11.8	23.6	47.1
5,000	3.000	106	35.3	4.7	9.4	18.8
	1.500		70.7	9.4	18.8	37.7
6,000	3.600	106	29.4	3.9	7.9	15.7
	1.800		58.9	7.9	15.7	31.4
7,000	4.200	106	25.2	3.4	6.7	13.5
	2.100		50.5	6.7	13.5	26.9
8,000	4.800	106	22.1	2.9	5.9	11.8
	2.400		44.2	5.9	11.8	23.6

These times assume continuous motion throughout each row and do not take into consideration the time required to move the stage to each new row.

2.4 Reflective Positioning Performance

The TDI Continuous Scanning System uses reflective positioning to determine “crude” focus by profiling the surface topology of the MTP membrane substrate (the bottom glass or polymer surface). The Keyence LK-G15 laser displacement used to profile the surface is capable of tracking up to four surface reflections (index of refraction changes that indicate a change in substrate optical composition). For the continuous scanning system, the first and second surfaces of the membrane were tracked. The first reflection represents the air-to-membrane interface. The second reflection represents the membrane to cells/fluid interface or biological specimen plane. The LK-G15 sensor is located 46.5 mm to the right of the center of the TE2000-E optical axis. The decision to place the sensor with this offset was due to the physical dimensions of the LK-G15, ease of placement on the Nikon microscope, and because it affords the ability to have a substantial look-ahead to pre-profile the surface topology before having to place the specimen in the “best” focal plane. A-priori information of surface topology helps ensure that the specimen will be at the correct focal plane at the exact time the specimens XY position is right over the objective.

Due to the physical placement of the sensor when scanning the MTP, the surface profiling begins at the laser-offset position and our scan length is increased to 147 mm per row as opposed to the 106 mm. This increase in distance increases the expected total scan time by 38%. With this added time,

the entire time required to scan a 384 well MTP at 20x objective magnification, 1.075x intermediate camera zoom, and line rate of 8,000 Hz is 16.3 minutes.

2.5 System Timing

The goal of this project is to scan over 100,000 wells per day at 10x and over 50,000 wells per day at 20x. With a 384 well plate scan time of just under 17 minutes using a 20x objective, we are able to scan 33,924 wells per day. At 10x, this count is 67,848 wells per day.

These scan times per plate don't take into consideration time to set up and / or remove a plate for scanning, time to move to the A01 position of the MTP and pre-focus to begin a scan, time to pre-profile, and the time to reset for each new row. This overhead accounts for an additional 20% to 30% of the total scan time. Using the hardware described previously at the maximum level of performance, it is seen that we will be unable to get to 100,000 wells per day at 10x or 50,000 wells per day at 20x. We are able to get just over half of the desired 50,000 wells per day at 20x, with a total of 26,141 wells. This translates to 68 384-well microtiter plates.

Chapter 3: *Software Development - Hardware Control*

Section Overview: Develop Software Control and Incorporate Robotics to Control System for stand-alone operation

3.1 Software Programming

- ***C++, C#, Labview, Matlab***

A 64-bit application capable of driving the TDI-CS System and incorporating robotic handling to allow for a true HT-HCS platform was created.

The controlling software was developed using C#, pronounced c-sharp, a Microsoft .NET framework programming API known for it's fast Graphical User Interface design time and robust and fast operational performance. C# was chosen for it's ease of programming, and because of the availability of native hardware drivers support. When developing software, platform independence is always a nice goal, however many manufacturers only provide Windows OS based drivers so using a Windows-centric programming language extends the ease of program development. The programming environment was in Visual Studio 2010 Express Edition (Microsoft).

The controlling software incorporates novel multi-threaded programming motifs to ensure fast and robust performance and will also utilizes GPGPU techniques to remove tedious and processor intensive per pixel calculations from the CPU and have the graphics board, which is better suited at performing tedious per pixel calculations simultaneously, process the calculations

Examples include:

- Calculating 2D autofocus on a through-focus stack
    - Performs fast 2D image convolution with filter capable of extracting mid to high spatial frequencies from each image.
    - The image with the highest spatial frequency translates to the best focus image.
- Adjusting gain and contrast in an acquired image for display
- Converting between bit depths for real-time image display
    - Scientific grade images are between 8 and 16 bits per channel per pixel (8, 10, 12, 14, and 16). All graphics displays are only capable of displaying 8 bits per channel per pixel (usually 32-bit, 4 channels - RGBA).

For robotic control, a Peak Robotics, Inc. Kinedx Robot and a Thermo-Scientific Cytomat Plate Hotel with plate shuttle was integrated to create a HT-HCS platform capable of scanning at a minimum of 189 standard size 384- well microtiter plates in a 24-hour period.

The TDI continuous scanning system uses a Dell dual Xeon quad-core server with 20 GB of memory, Windows 7 x64 as the OS and over 3 TB of hard drive storage as the controlling PC. The storage comprises a 250 GB drive for the main OS drive, four 15000 rpm 250 GB Serial-Attached-SCSI (SAS) drives combined in raid-0 to create a 1 TB drive for an image capture drive, and a 2 TB

drive as image storage drive. The TDI-CS System requires massive storage and high bandwidth drives to handle the fast read and write speeds, between 80 MB/s and 250 MB/s, and because of the large data sets captured with every MTP scanned.

Each strip (the entire row of a 96, 384 or 1536 well plate) will encompass approximately 106mm. Depending on magnification, this translates to around 170 @ 10x or 340 @ 20x images per strip. As mentioned previously, each individual image captured by the C7780-51 is 8.257 MB. Each strip then requires approximately 1.4 GB @ 10x to 2.8 GB @ 20x of hard-drive storage. With a large memory buffer (~3 GB), the program is able to store the images captured in TDI mode in memory to avoid missing frames due to unforeseen disk I/O problems. Once a strip is captured however, multithreaded disk I/O writes the memory stream to disk in under 14 seconds or approximately 200 MB/s.

The drivers for the various hardware peripherals include Hamamatsu's DCAMAPI suite, a custom TE2000E driver built around Nikon's RS-232 serial command set, a custom Lumencor Aura driver built around Lumencor's RS-232 serial command set, National Instruments data acquisition and output driver, DAQmx, and National Instruments motion control driver, FlexMotion32. The DCAMAPI, DAQmx, and custom serial command based drivers all natively support 64-bit operating environment. FlexMotion32 is however limited to only 32-bit. As mentioned before, the TDI continuous scanning system software is a

64-bit application that has a 3 GB dynamic ring buffer to store images as they arrive from the camera. 64-bit applications have different memory instructions when compared to 32-bit applications and they also require and run in a different application domain. This means that if you have a 32-bit driver, it can only run in a 32-bit environment and the same goes for a 64-bit driver. To get around this and have a 64-bit program control a 32-bit driver, I created a 32-bit server application that uses named pipes to allow communication between a 32-bit process and a 64-bit process.

3.2 Software Description

The following sequence of images walk you through how the software is launched and run for a typical scan:

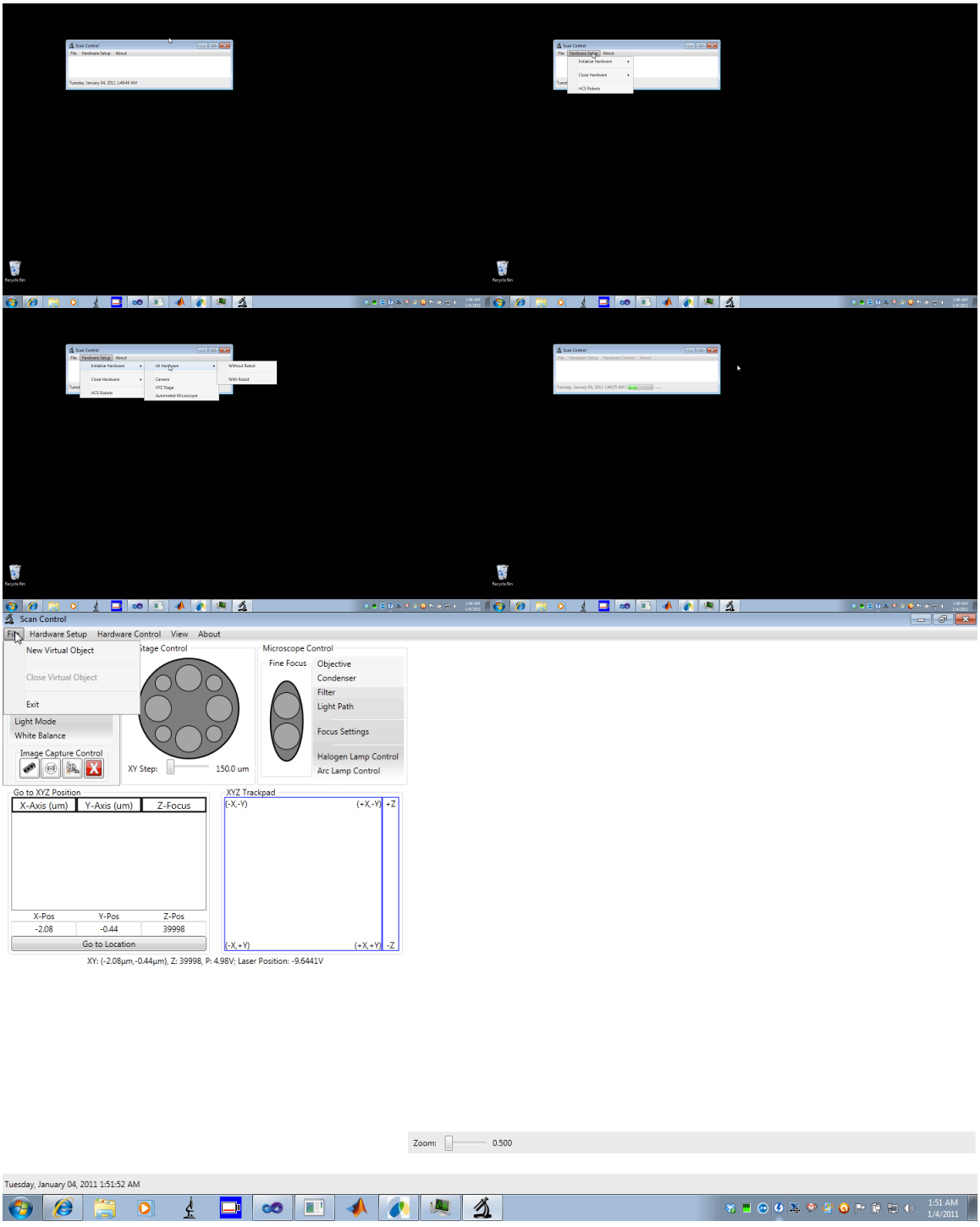

Figure 3.1: Desktop screenshots showing the launch and initialization of the TDI-CS System.

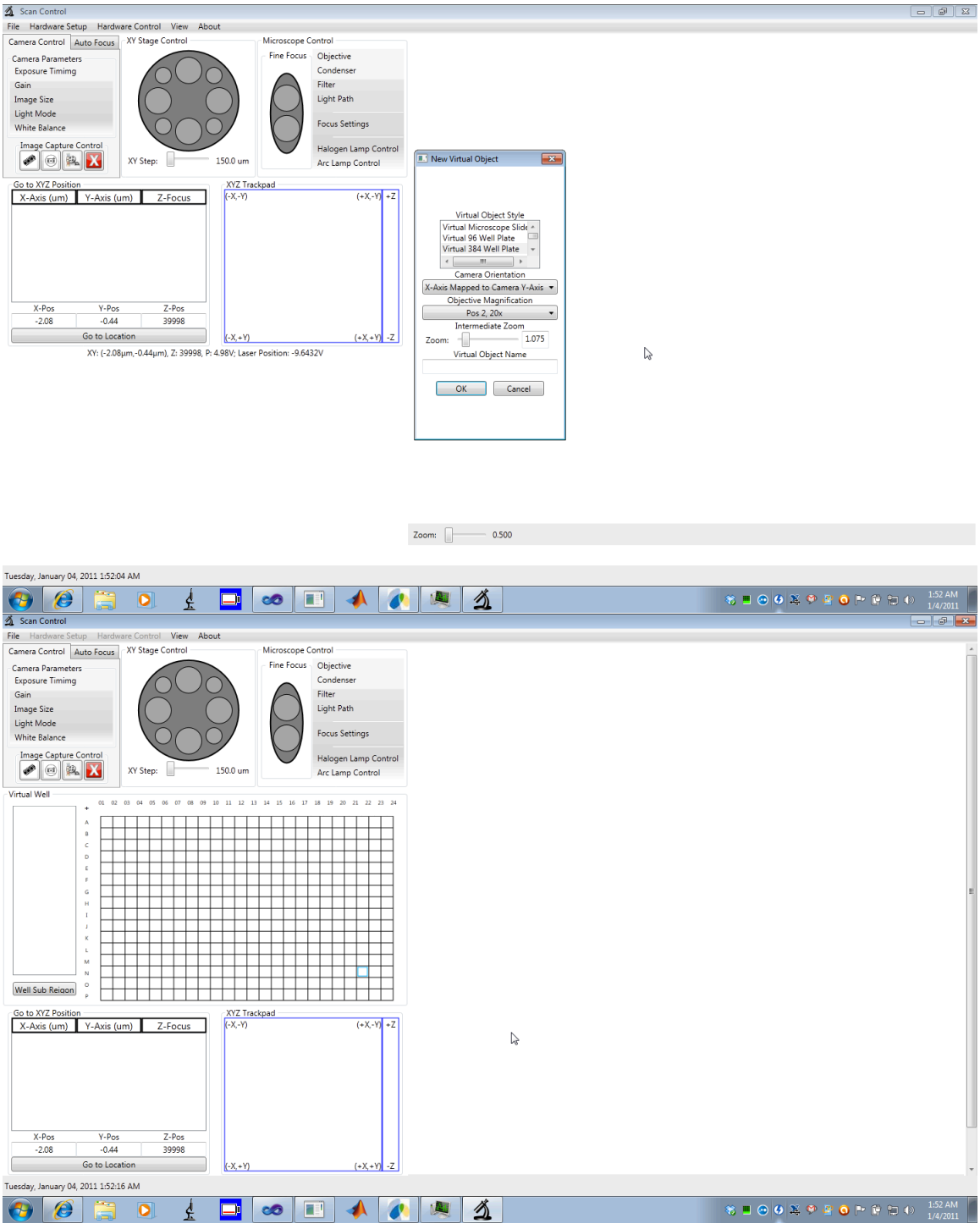

Figure 3.2: Desktop screenshots showing the creation of a “virtual” microtiter well plate that represents the physical MTP to be scanned by the TDI-CS System.

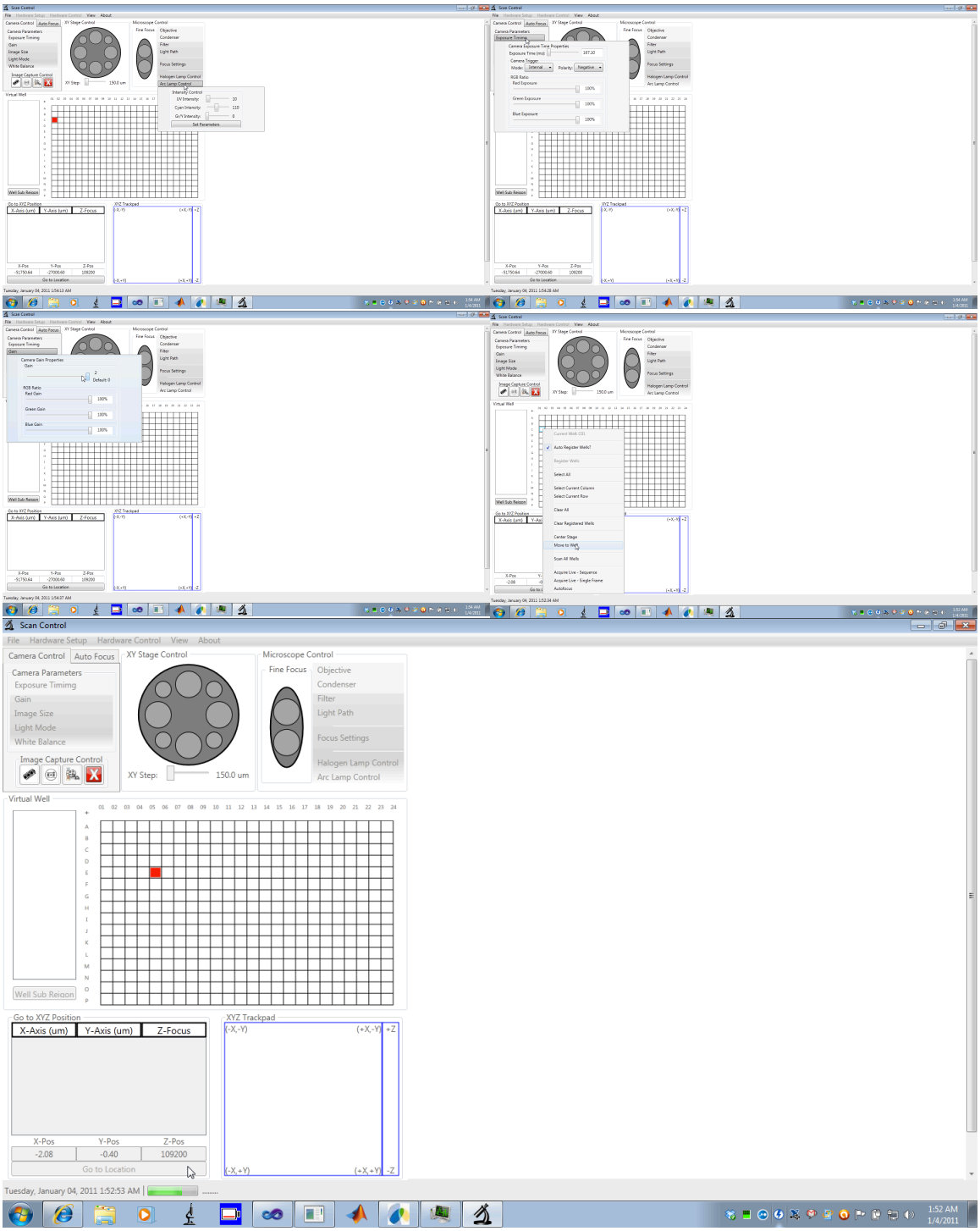

Figure 3.3: Desktop screenshots showing the basic functionality of the TDI-CS software suite. The user can control XY Stage Position; Camera parameters such as Exposure Time, Gain, Image Size; Microscope parameters such as Condenser, Filter, Light Path, Objective, Focus Nose Piece Position, Arc Lamp and Halogen Light intensity

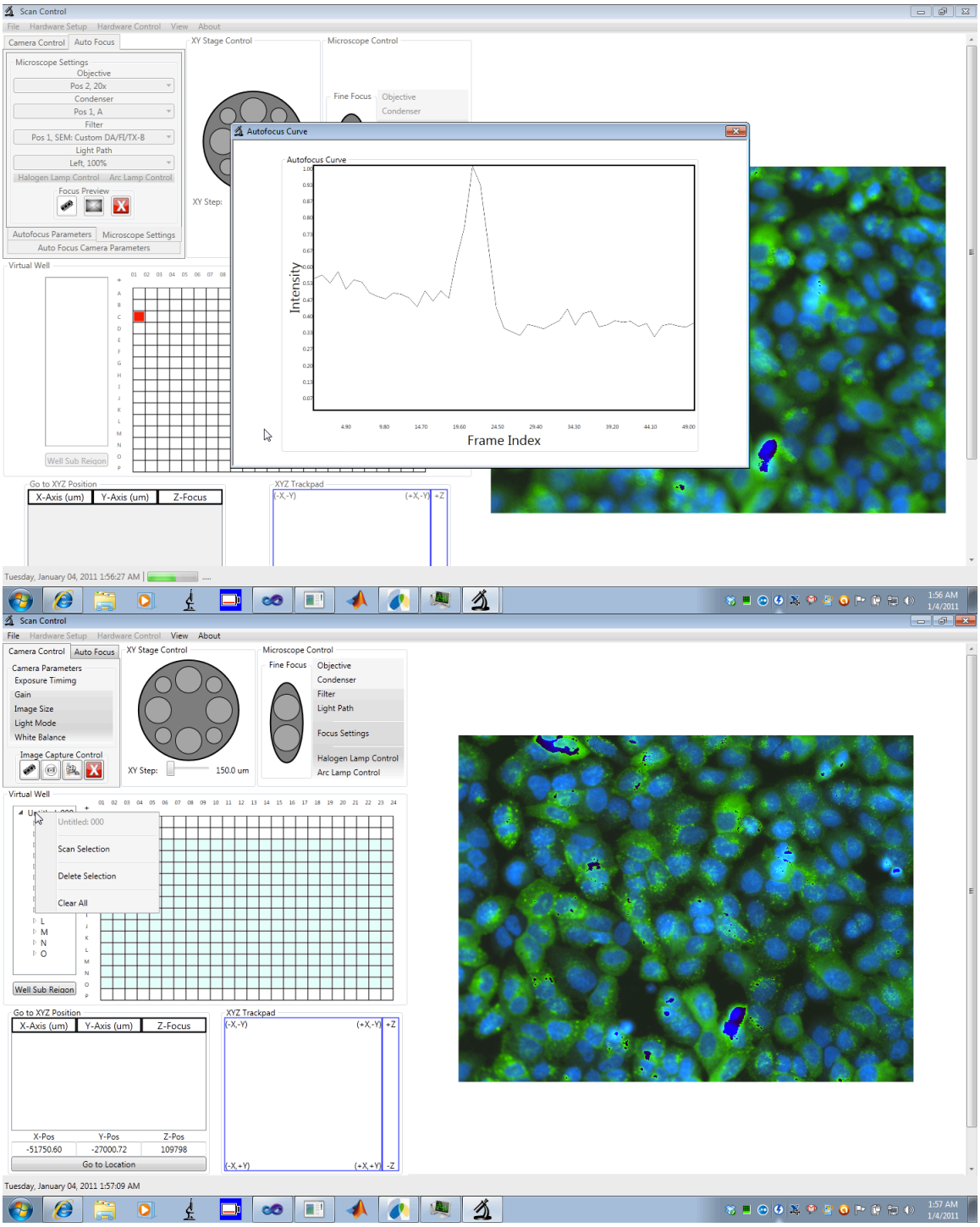

Figure 3.4: Desktop screenshots showing the results of an image based Autofocus routine of a GPR55 assay plate

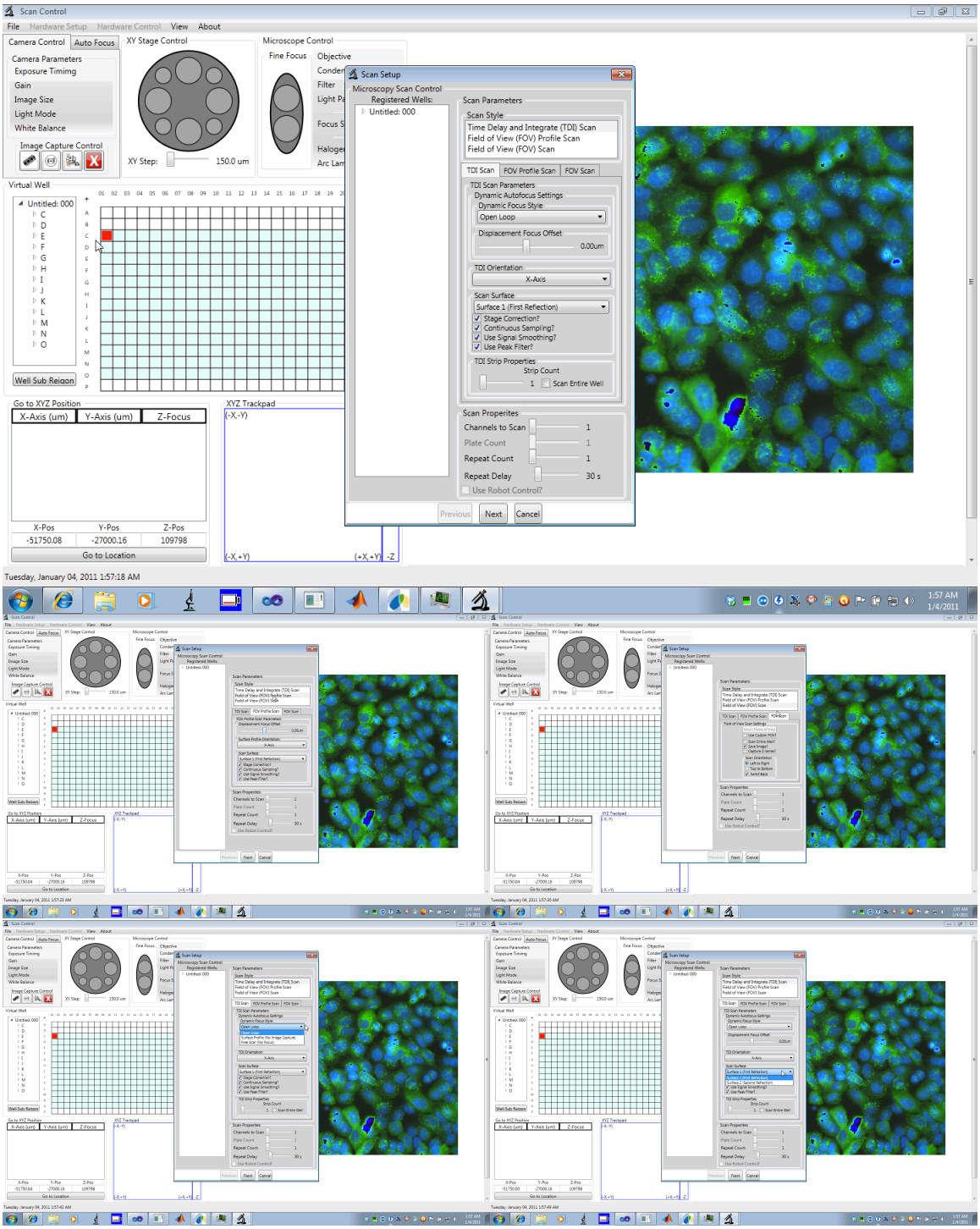

Figure 3.5: Desktop screenshots showing the setup of a Plate Scan using TDI image capture and surface profiling for dynamic reflective positioning based focus

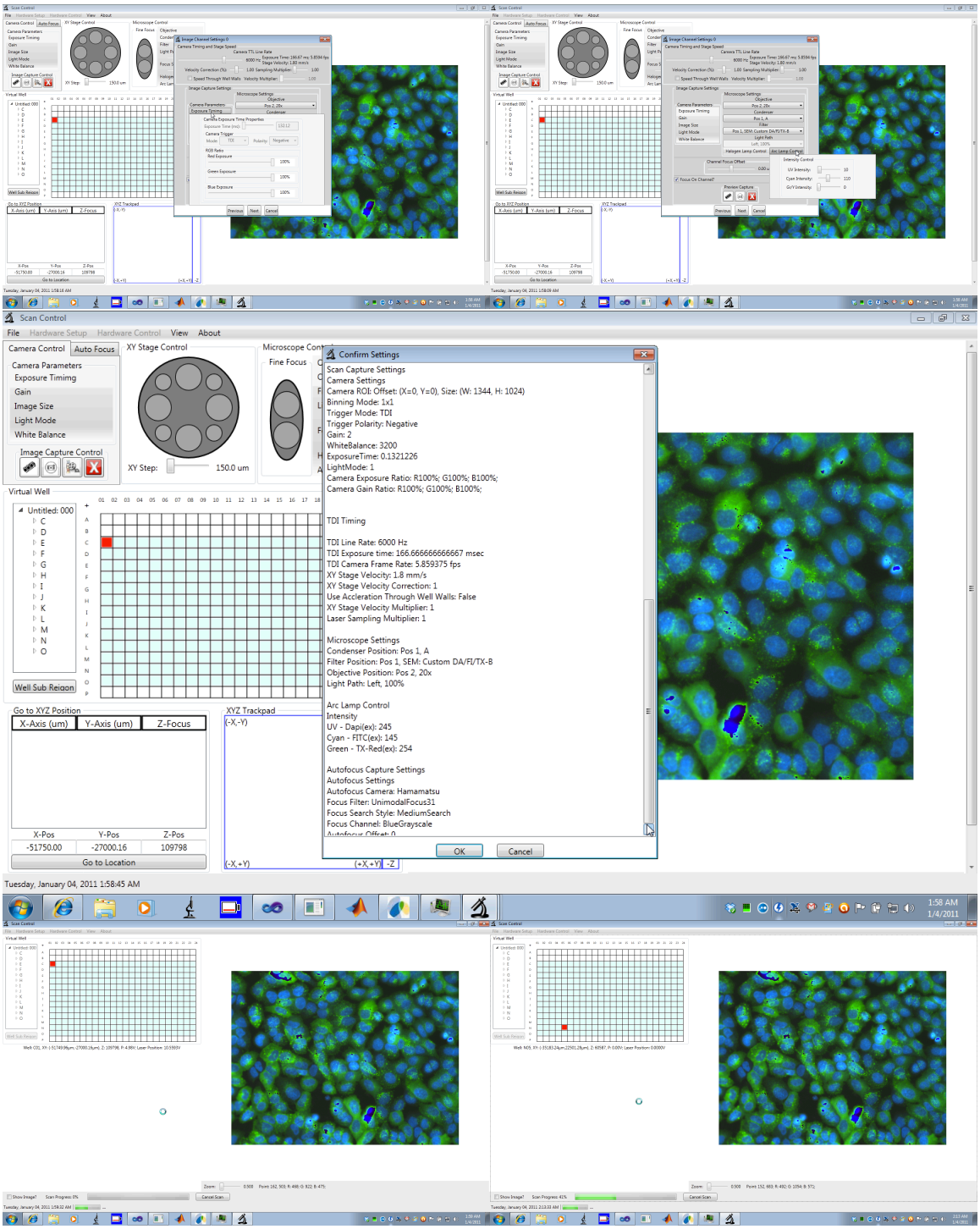

Figure 3.6: Desktop screenshots showing the setup of a Plate Scan using TDI image capture and surface profiling for dynamic reflective positioning based focus

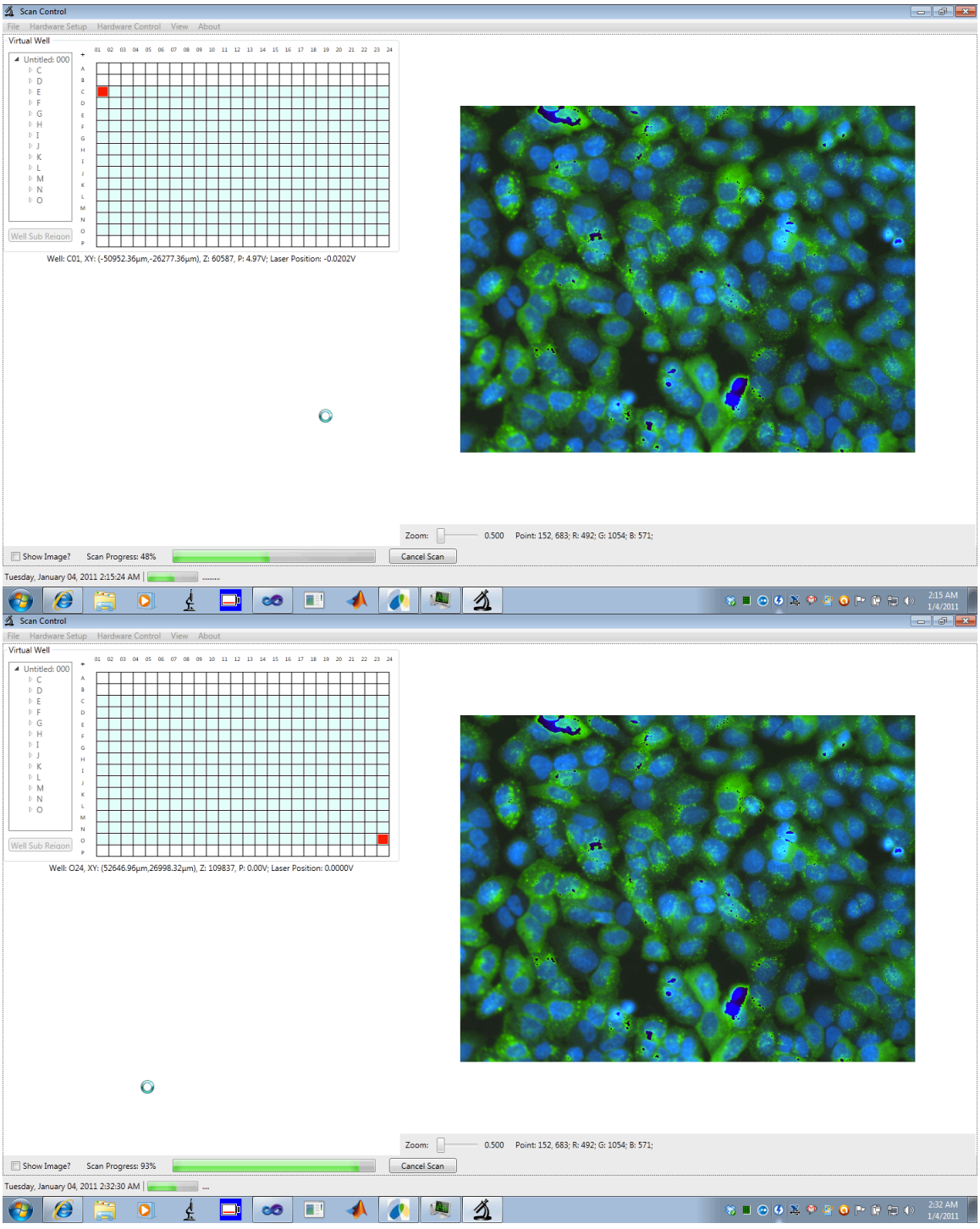

Figure 3.7: Desktop screenshots showing the progress of the scan

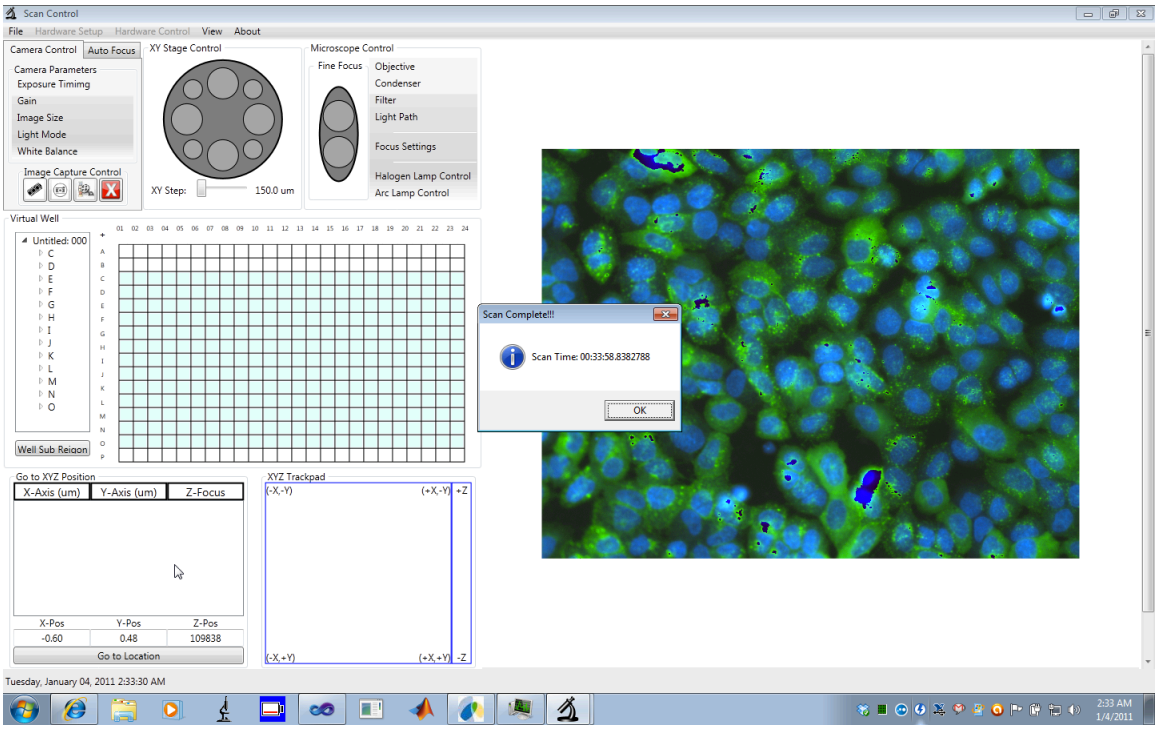

Figure 3.8: Desktop screenshots showing the completion of a plate scan and the time associated with capture

Chapter 4: *System Testing and Validation*

Section Overview: Characterize System Performance Qualitatively and Quantitatively using control assay and biological assays being screened at the Sanford-Burnham Center for Chemical Genomics.

Assays for System Characterization

- ***Ronchi Ruling Grid***
- ***Biological Assay***

The goal of the TDI-CS System is to increase image capture bandwidth associated with HCS experiments using 384 and 1536 well plates. A system that uses Time Delay and Integrate (TDI) imaging as well as dynamic autofocus was designed and developed using off-the-shelf commercially available hardware.

Materials & Methods

In order to test the performance of the TDI-CS System, a Ronchi ruling grid was first used to make quantitative measurements of resolution and out of focus blur. Further validation for the TDI-CS System performance was done by comparing assays screened in the Sanford Burnham Institutes Chemical Genomics Screening Center using their core facility HCS Instrument, the Perkin Elmer Opera. Once scanned, the assay plate data is analyzed using Vala Sciences' CyteSeer, a cell based image-processing program that automatically segments and scores the image data based on nuclear dna content, cellular

morphology and many other parameters. Comparing the data analysis between a plate scanned from the TDI-CS System and the same plate scanned using the screening systems HCS Instruments will provide a direct relationship between the differences in image quality for the respective systems. The commercially available HCS systems will be used as the golden standard.

4.1.1 Synthetic Target

A *Ronchi Ruling (RR),* also called a Ronchi *grating* is a constant-interval square wave optical target that has a high edge definition and contrast ratio. Ronchi rulings are used for optical testing purposes[19].

Figure 4.1: Graphic showing example of a Ronchi Ruling. The sharp edge definitions for the dark to light transition of the square wave provide an excellent resolution target for MTF measurements.

We used a Ronchi ruling to track the performance of the TDI-CS System as a function of spatial (XYZ) location. A SBS standard MTP has an area footprint of 127.76 mm x 85.48 mm and an active scanning region of about 106 mm x 75 mm. In order to model this region, we purchased a custom Ronchi ruling

grid (Applied Image, NY) that has same footprint as a MTP, an active imaging area of 102 mm x 75 mm, and a square wave frequency of 20 cycles per millimeter.

With this synthetic target, we are able to test the ability of the Keyence sensors ability to track and maintain optimal focus as well as track linear motion blur associated with continuous stage motion while performing Time Delay and Integrate image capture.

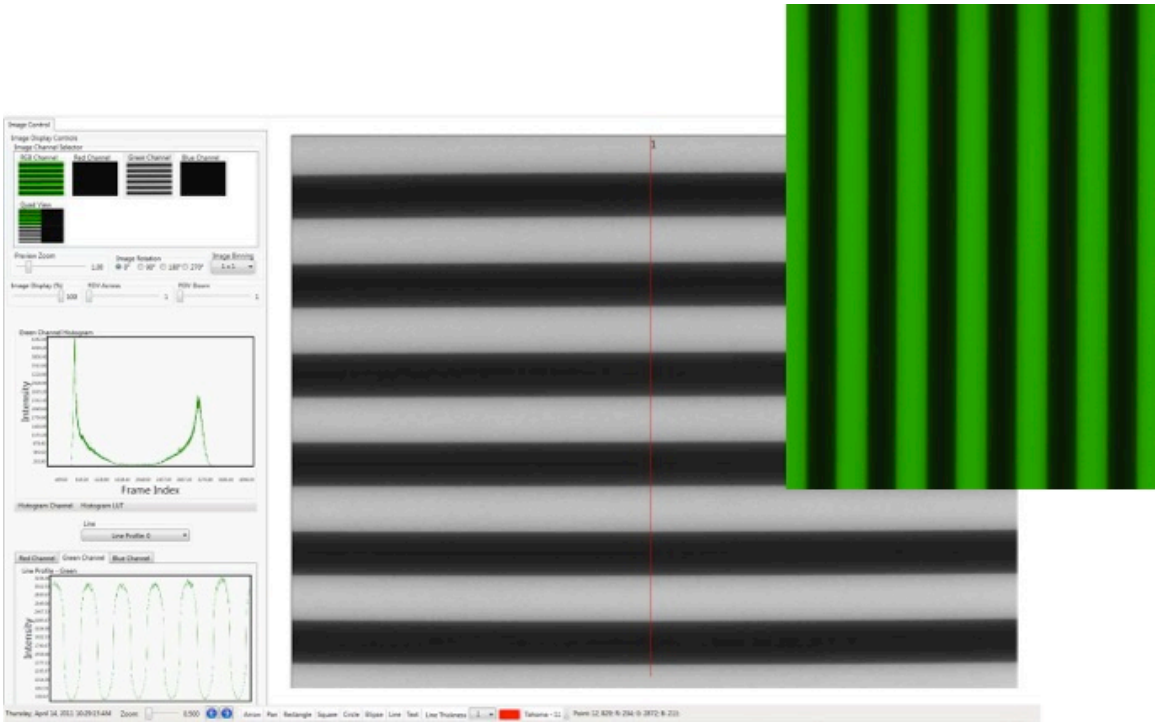

Figure 4.2: Image of Ronchi Ruling grid captured by the TDI-CS system. Custom software allows user to select a line profile of the image and displays the histogram and profile intensity.

4.1.2 Stage Calibration

Due to the 46.5 mm offset of the Keyence sensor from the optical axis, there is potential for tilt or cantilevering associated with stage travel to be present in the surface profile measured by the Keyence sensor. This translates to not tracking the Ronchi Ruling surface correctly.

We performed stage calibration to ensure the laser displacement information given by the Keyence sensor is representative of the best focus position of the target specimen as seen through the objective lens.

In order to account for the positional offset, we scanned the Ronchi ruling grid in two modes. First, image based focus was performed over the entire scanning area of the grid. Using the 31-tap convolution filter to find best Z-focus, we recorded the position of the objective nosepiece a function of the XY stages position[9-13]. The active area of the grid was scanned in a snake-like raster pattern and we performed a through focus stack every 1 mm going from left to right and top to bottom. From this, we generated a surface topology profile map of the Ronchi ruling grid based on best image focus. We then scanned the same active area of the Ronchi ruling grid and monitored the Keyence sensor's displacement. Using the NI DAQ board, we sampled the Keyence sensors output at 25,000 Hz while moving the XY stage from left to right 102 mm at a velocity of 1.8 mm/s. We did this with a pitch of 1 mm as the stage traveled down the 75mm height of the Ronchi ruling in the Y-axis direction. Once complete we generated a surface

topology map of the Ronchi grid based on laser displacement. The laser displacement sensor outputs an analog voltage signal ranging from -10 V to 10 V. This voltage represents a +/- 1 mm change from the sensor's nominal position. We programmed the Keyence sensor to output a displacement reading after averaging 16 samples. The sampling rate of the displacement sensor is 50 kHz or 50,000 samples per second. This makes the sensor's effective sampling rate 3,125 Hz.

To generate the surface topology map from the laser displacement voltage data, we decimated the data by averaging every 250 samples and then

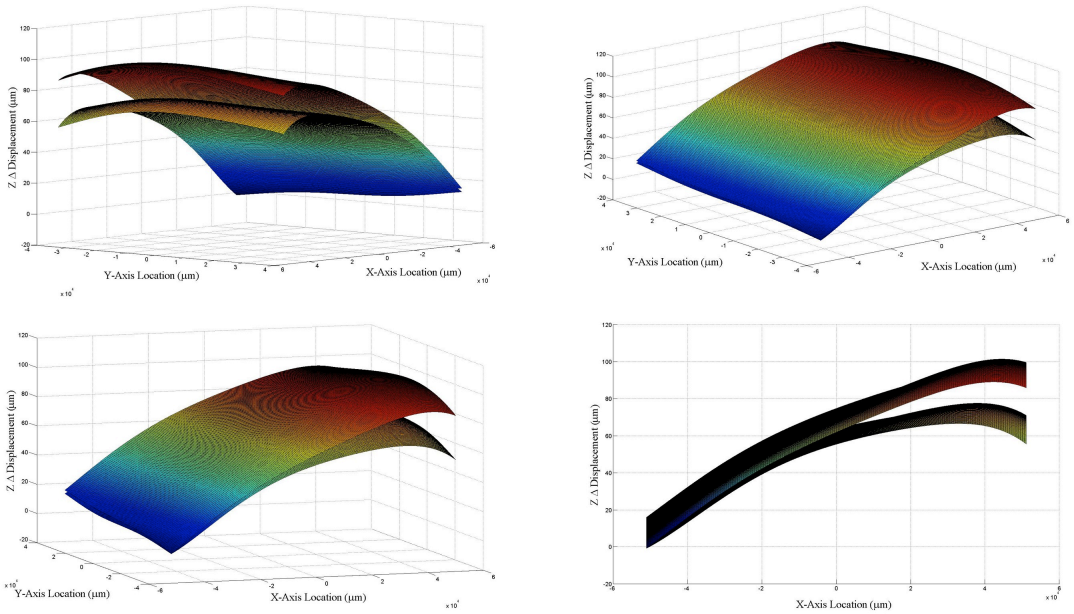

Figure 4.3: Surface Profile plots showing the Image Based Focus derived RR surface topology map and the Reflective Positioning derived RR surface topology map

determined the delta displacement between the initial displacement position and every other position collected.

Once captured, we used Matlab's curve fitting toolbox functionality to turn our surface topology data points gathered for the Ronchi ruling (from both tracking modes) into functions of stage position Z = F(x,y). This allowed us to then subtract the image based surface map from the reflective positioning surface map to get the Z-offset distance between the "true" surface topology profile and the profile generated using our laser displacement sensor. We then

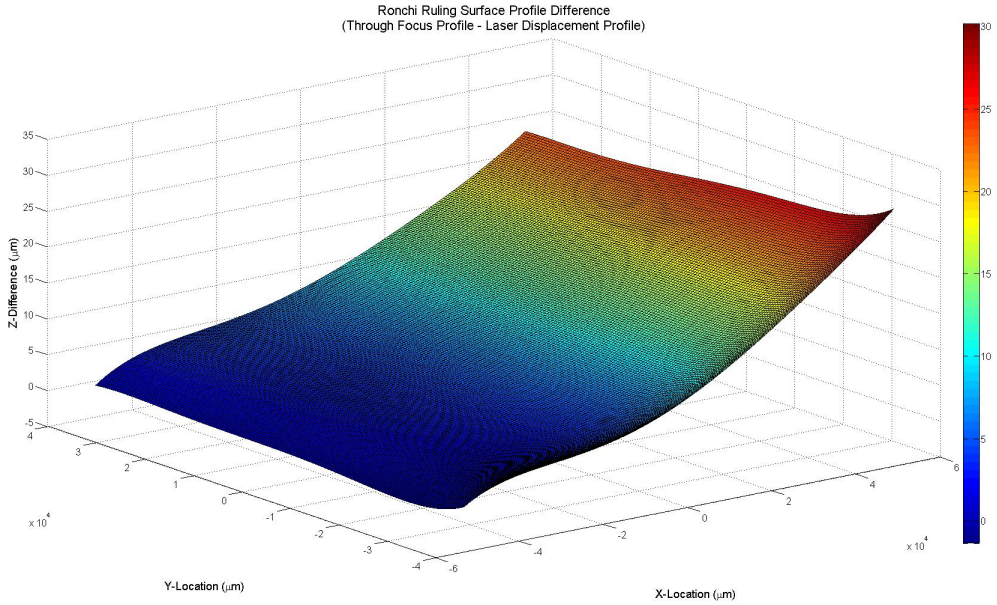

Figure 4.4: Surface topology map of the difference between the Image Focus based RR surface profile and the Reflective Positioning based RR surface profile

used the curve fitting toolbox to create a 5th order polynomial surface fit representative of the offset distance in Z as a function of the stages XY position.

Using the correction factors generated from the polynomial fit, we should be able to ensure that any tilt or cantilever induced Z-offset associated with the Keyence sensors physical mounting position will be removed from the surface topology map generated by the Keyence sensor.

Table 4.1: The following represents the 5th Order Polynomial Fit generated using Matlab's Curve Fitting Toolbox:

Z(x,y) = p00 + p10*x + p01*y + p20*x^2 + p11*x*y + p02*y^2 + p30*x^3 + p21*x^2*y + p12*x*y^2 + p03*y^3 + p40*x^4 + p31*x^3*y + p22*x^2*y^2 + p13*x*y^3 + p04*y^4 + p50*x^5 + p41*x^4*y + p32*x^3*y^2 + p23*x^2*y^3 + p14*x*y^4 + p05*y^5

x: Normalized by mean = 0 and std = 2.959e+004; (X - 0) / 2.959e+004

y: Normalized by mean = 0 and std = 2.208e+004; (Y - 0) / 2.208e+004

X: Stage Location along the X-Axis in microns

Y: Stage Location along the Y-Axis in microns

Polynomial Coefficients (with 95% confidence bounds):

- p00 = 0.1493 (0.1493, 0.1493)
- p10 = 0.1425 (0.1425, 0.1425)
- p01 = 0.006686 (0.006686, 0.006686)
- p20 = 0.06123 (0.06123, 0.06123)
- p11 = -0.01652 (-0.01652, -0.01652)
- p02 = -0.01163 (-0.01163, -0.01163)
- p30 = -0.01373 (-0.01373, -0.01373)
- p21 = -0.009458 (-0.009458, -0.009458)
- p12 = -0.001216 (-0.001216, -0.001216)
- p03 = 0.01036 (0.01036, 0.01036)
- p40 = -0.009254 (-0.009254, -0.009254)
- p31 = 0.00124 (0.00124, 0.00124)
- p22 = 4.016e-005 (4.016e-005, 4.016e-005)
- p13 = 0.0008357 (0.0008357, 0.0008357)
- p04 = 0.006358 (0.006358, 0.006358)
- p50 = 0.00527 (0.00527, 0.00527)
- p41 = 0.0007449 (0.0007449, 0.0007449)
- p32 = 0.0005922 (0.0005922, 0.0005922)
- p23 = 0.0005532 (0.0005532, 0.0005532)
- p14 = 0.000427 (0.000427, 0.000427)
- p05 = -0.004713 (-0.004713, -0.004713)

4.1.3 Resolution Quantification

In order to test the positional accuracy of the displacement sensor with our newly developed stage correction factor, we scanned the Ronchi ruling surface using the reflective positioning technique described previously. Once the scan for surface topology was complete, we went to each (X,Y) coordinate available within the active area of the Ronchi ruling grid on a 1mm pitch and adjusted the Z-position of the piezo stage according to the surface maps specification "Z = F(x,y)" and captured a full frame, static 2D image. Following image capture, we performed visual inspection to see how "in focus" each image was and quantitatively compared the surface profile generated images to the images captured using image-based focus.

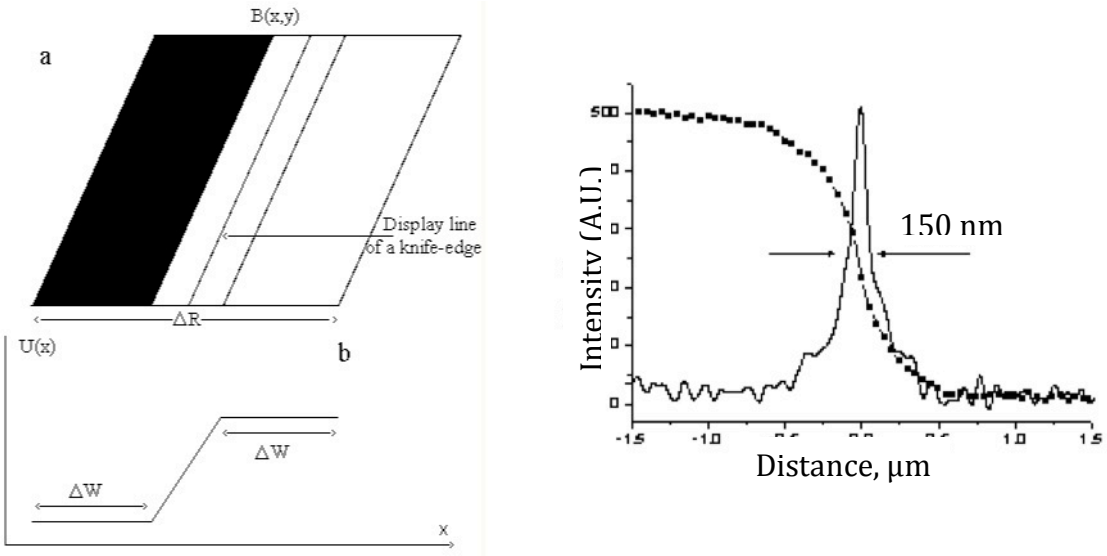

Figure 4.5: (a) Schematic showing knife-edge (b) corresponding intensity profile of a cross-section (c) Line profile of edge function and corresponding Gaussian fit and outline of the FWHM

To quantitatively assess the differences between the static images captured using image-based focus versus using surface profiling we performed knife-edge resolution analysis. Knife-Edge analysis is a correlative measure to the MTF of an optical system including the imaging detector. For our analysis the quantifiable metric we use is how many pixels are required to capture the transition from dark to light on our Ronchi Ruling. As mentioned before, the Ronchi grid has a high contrast square wave pattern that transitions from dark to light at frequency of 20 cycles per mm. This transition is expected to be very sharp and should thus require very few pixels.

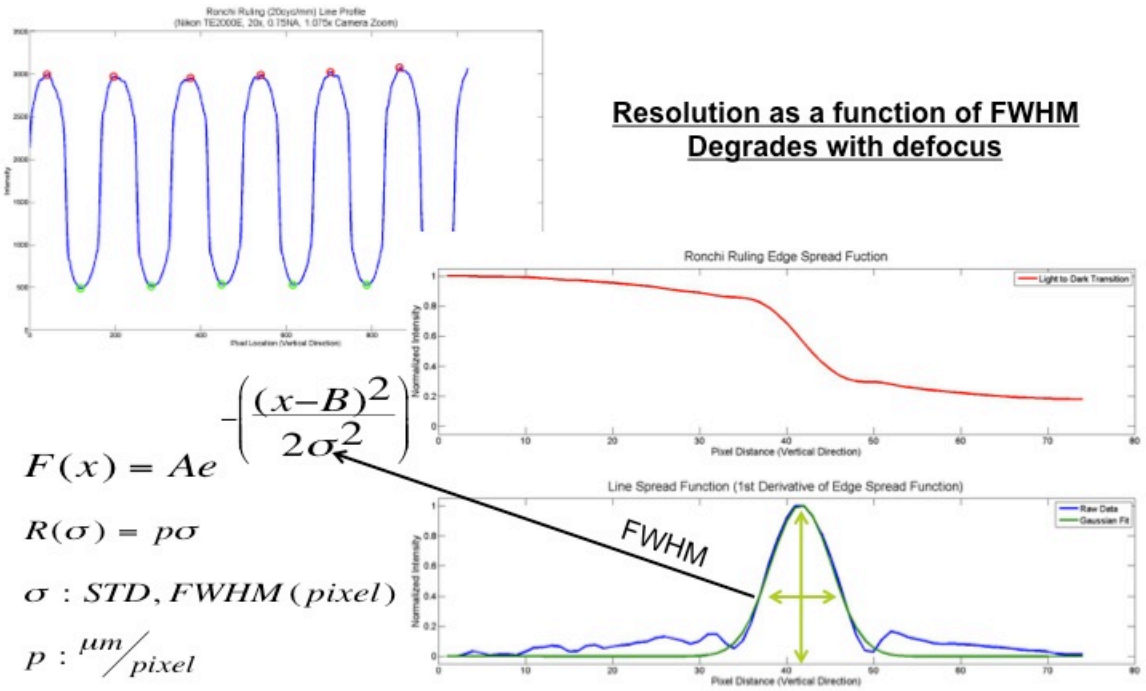

Figure 4.6: Graphic showing plots of the line profile, edge spread function, and line spread function from an image of the Ronchi Ruling grid used. Custom software automatically determines the min and max points on the line profile, segments each min/max pair in sequential order, calculates the 1st derivative to find the "Zero-Crossing", and performs the Gaussian fit to determine the Full Width Half Maximum.

To perform this analysis custom code was written in Matlab. The software extracts a line profile of the image, takes the 1st derivative of the line profile, and then fits the resulting derivative to a Gaussian fit. The coefficients from the Gaussian fit provide the information needed to extract the resolution measurement in pixels. This value is then multiplied by the effective µm/pixel size

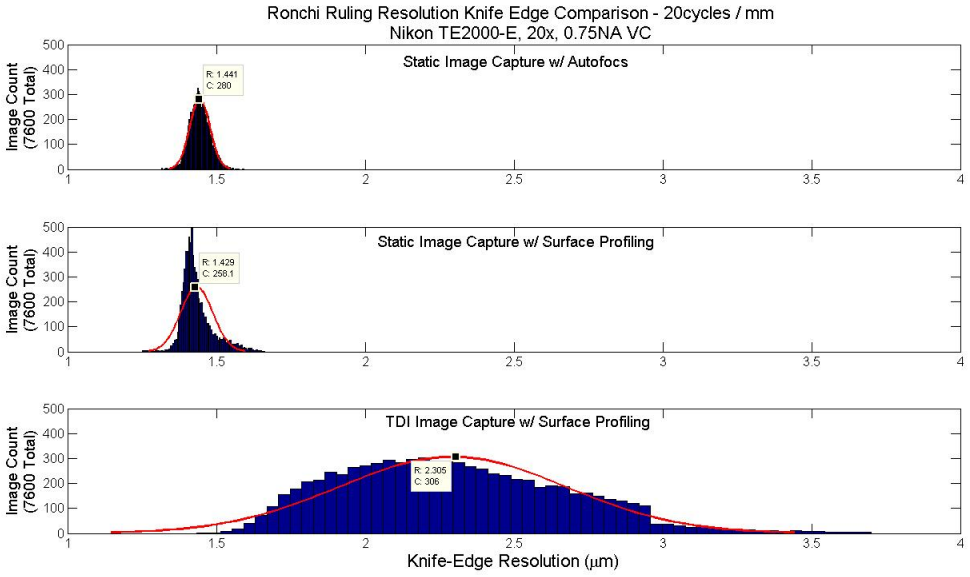

Figure 4.7: Graphs showing comparison of the histogram fit of knife-edge resolution measurements on images captured using: Static Image capture using autofocus, Static Image capture using surface profiling, and TDI Image capture using surface profiling

of our imaging system to provide our resolution measurement in terms of a length measurement[20-23]. The results from the image analysis showed the average distance to go from the dark to light region of the Ronchi grid for the static images captured using image based focus was 1.44 ± 0.034 µm or approximately 4.8

pixels and the average distance for the static images captured using surface profiling was 1.43 ± 0.054 µm or approximately 4.77 pixels. All images used for the comparison were captured using a 20x, 0.75 NA VC objective and a 1.075x camera zoom, on a Nikon TE2000-E microscope with transmitted light (halogen lamp was set to 233 or 91.4% of its maximum intensity). A FITC HQ:F filter was used to provide a single color spectrum. The HQ:F filter provides excitation of 480/40 and emission of 535/50. The C7780-51 TDI camera was set to image in area scan mode with 1x gain and an exposure time of 170ms.

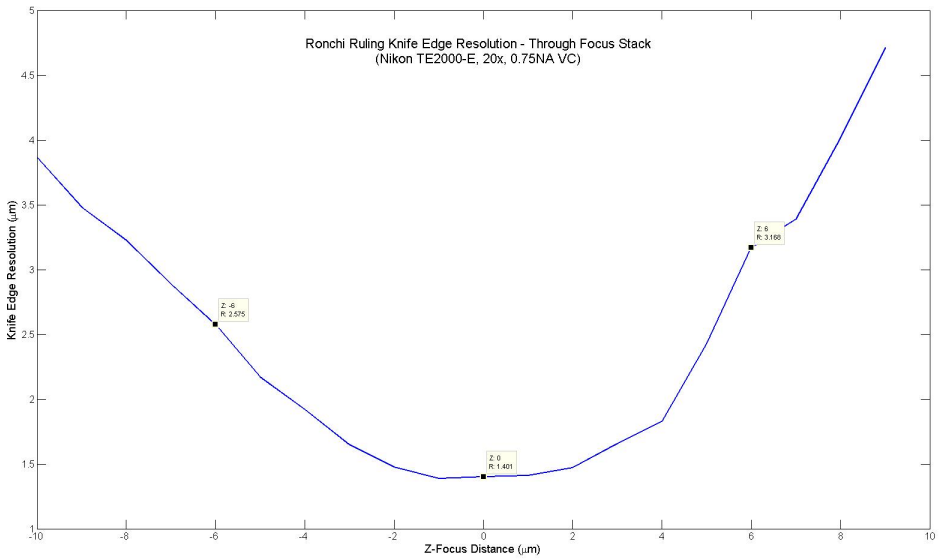

Figure 4.8: Graphs showing Knife-edge resolution measurements on a through focus stack as a function of de-focus distance from best focus

We also captured a through focus stack of the Ronchi grid and performed the same knife-edge resolution measurement on each image in the stack to get a resolution measurement as a function of de-focus distance. From the results, we found that the static images captured using image based focus and reflective

positioning were ± 0.75 microns from each other and well within the depth of field of the 20x, 0.75 NA VC objective used. The depth of field for the 20x objective was found to be approximately 0.95 ± 0.05 µm, assuming a wavelength of 535nm and an e of 1µm.

$$d_{tot} = \frac{\lambda * n}{NA^2} + \frac{n}{M * NA} * e$$

d_{tot} = Depth of Field

NA = Numerical Aperture

M = Magnification

e = Smallest distance able to be resolved by the detector

λ = Wavelength of light

n = Index of refraction

The Ronchi ruling grid helped us to ensure that we are able to effectively monitor and track the changes in surface topology using the Keyence laser displacement sensor. We are able to get a pre-profile of the surface of our 384 well MTP and image the regions of interest in each well while maintaining a suitable level of focus without the need to perform image based autofocus. Using reflective positioning alone, the scan time required to image an entire 384 well dish dropped by a factor of 4.

4.1.4 TDI Image Capture

Using the Ronchi Ruling grid, we have proved that we are able to maintain optimal focus of our target specimen without having to perform image-based focus under static conditions, i.e., all image capture is done while the XY stage is not moving. The goal of the TDI-CS system is to capture the HCS data with stage motion to increase the bandwidth of data capture. It is known that capturing images of moving objects under normal imaging modalities will cause sever image artifact due to motion blur.

Time Delay and Integrate imaging helps minimize (if not completely remove) motion blur artifact by synchronizing image capture with the velocity of the moving object. The TDI-CS system uses the linear encoder TTL positional feedback to synchronize and trigger image capture from TDI camera. As long as the velocity of the stage is within 4% of the expected vertical line rate of camera, images should be captured without motion blur. To test how much artifact is introduced in the images due to motion blur, we compared images captured using static imaging with TDI imaging.

The Ronchi Ruling grids active area (102 mm x 75 mm) was scanned in TDI mode using the same microscope settings that were used in static image capture mode. We used same 20X, 0.75NA VC objective, HQ:F filter cube, and maintained the same halogen lamp intensity for transmitted light capture. Under static image capture, the C7780-51 TDI camera's exposure time was set to 170

milliseconds. To create this effective exposure time in TDI mode requires a vertical line rate of 6000 Hz. The C7780-51 has 1024 vertical lines, which all behave as an integration stage for photoelectrons. Each vertical line therefore collects 1/6000s or 166.7 microseconds worth of photoelectrons to give an equivalent exposure time of 170.6 milliseconds. At 20x magnification with 1.075 camera zoom, our TDI camera's effective pixel size is 0.3 μm/pixel. With this effective pixel size, the XY stage holding our Ronchi Ruling grid must maintain a velocity of 1.8 ± .07 mm/s.

For our experiment we first pre-profiled the Ronchi Ruling grid using the same sampling parameters we did when performing static image capture with surface profiling. The stage scanned the full 102 mm x 75 mm with a 1mm pitch in the Y-direction at 1.8 mm/s. The NI-DAQ board sampled the laser displacement information at 25,000 Hz during stage motion and we then decimated the resulting profile down by averaging every other 250 samples. We then scanned the active area of the Ronchi Ruling grid with the stage traveling at 1.8 mm/s. During stage motion we provided an analog voltage ranging from ± 10V to our 500 μm travel piezo stage. The analog voltage corresponds to the offset position between the surface profile measured by the laser displacement sensor and the best-predetermined focus position. The analog voltage output was synchronized to the stages position and the data was applied at a rate of 100 Hz. Performing this dynamic motion of our piezo stage enabled us to capture

images using TDI while maintained “crude” focus as determined by the reflective positioning sensor.

As mentioned before, we compared static images captured using image based focus and reflective positioning using Knife-Edge resolution measurements. This comparison showed that reflective positioning could successfully track best focus. Using the same analysis approach we compared the knife-edge resolution of the images captured in TDI mode versus images captured in static mode based on the reflective surface profile. Any changes found in resolution will be due to motion blur. The results from the knife-edge analysis showed the showed the average distance to go from the dark to light region of the Ronchi grid for the TDI images captured using surface profiling was 2.36 ± 0.48 µm or approximately 7.67 pixels. From the resolution versus de-focus distance analysis performed, it is seen that a resolution of 2.30 µm translates to a de-focus distance of ± 4 µm.

Table 4.2: Chart Showing scan type, image count, and average resolution with standard deviation

Scan	Image Count	Resolution (µm)
FOV	7638	1.44 ± 0.03
FOV Profile	7691	1.43 ± 0.06
TDI	24852	2.36 ± 0.48

Results from the knife-edge analysis show us that we are just outside of the depth of field of the 20x VC objective when using TDI and dynamic focus. The culprit behind our inability to match resolution could be our stepper motor driven stage. Stepper motors are famous for providing outstanding submicron positional accuracy with their micro-stepping feature. They however, are notorious for being incapable of providing smooth continuous velocity when traveling from position to position. Because of this, we are not able to maintain the desired line rate of 6000 Hz at all times. The stage has dynamic and oscillating fluctuations in velocity as it travels at the desired 1.8 mm/s. The fluctuations range from 1.5 to 2.3 mm/s. Although these changes only last for fractions of a second, they could induce motion artifact on the time scale of the TDI camera vertical integration step. There is also a potential chance that the TTL signal derived from the linear encoder could have caused the motion artifact. Spurious pulses generated from the divide-by-n signal not conditioned properly would advance or delay the vertical integration stepping in the CCD camera and cause motion blur.

Another culprit for this loss of resolution could be the TDI camera itself. Most TDI cameras have a vertical line count of 16, 32, 64, 128, and traditionally a max of 256. Line counts greater than 256 can allow inherent electronic hardware error (noise, misaligned pixels, horizontal read-out error, …etc.) to show within each captured image. It is unfortunately, impossible to de-convolve electronic

noise and artifact generated from the camera itself, from the images captured using the TTL signal to advance the photoelectrons to each new line.

Biological Assay – Comparison between TDI-CS and the SBCCG's Perkin Elmer Opera

4.2.1 PML Oncogenic Domain

For the biological assay chosen to compare the performance of the TDI-CS system to a gold standard instrument used in the Sandford-Burnham Center for Chemical Genomics (SBCCG), the Perkin Elmer Opera, we chose the PML Oncogenic Domain Assay. This assay was performed in a Greiner 384-well MTP. PML is a multi-functional protein with roles in tumor suppression and host defense against viruses. When active, PML localizes to subnuclear structures named PML oncogenic domains (PODS). Inactive PML is located diffusely throughout the nucleus of cells. The objective of the SBCCG's study was to develop a high content screening (HCS) assay for the identification of chemical activators of PML.

To compare the image data captured using the Perkin Elmer Opera and the TDI-CS, we used Vala Sciences, CyteSeer, HCS image processing software to automatically segment the images and perform quantitative analysis on a feature set representative of good focus.

4.2.2 The Perkin Elmer Opera

The Perkin Elmer Opera is a robust HCS platform capable of multi-channel image acquisition. The system uses up to 4 dedicated laser lines. They

system uses spinning disk confocal microscopy to allow for fast exposure times, great optical resolution (>0.5NA) and lower background noise than that found in traditional fluorescence microscopy. The system also uses reflective positioning for best focus. However, the unit uses through the objective laser based focus. Typical throughput is around 38000 well per day or 100 384-well MTP.

4.2.3 Image Analysis

Metrics used to score the differences between the images collected from the TDI-CS system and the Perkin Elmer Opera were measurements that would quickly show the difference between an in-focus image and an out of focus image. Measurements such as average area of nuclei, roundness, and nuclei count were used.

Due to the roundness metric also including the area, I report here only the comparison of roundness.

$$R = \frac{4\pi A}{P2}$$

R: Roundness

A: Area

P: Perimeter

Objects that are round tend to become more elliptical and oblong in shape as they blur due to change of best focal plane and motion artifact. Comparing the roundness of nuclei is a great way see how well the TDI-CS system was able to capture nuclei and not have them subjected to motion blur.

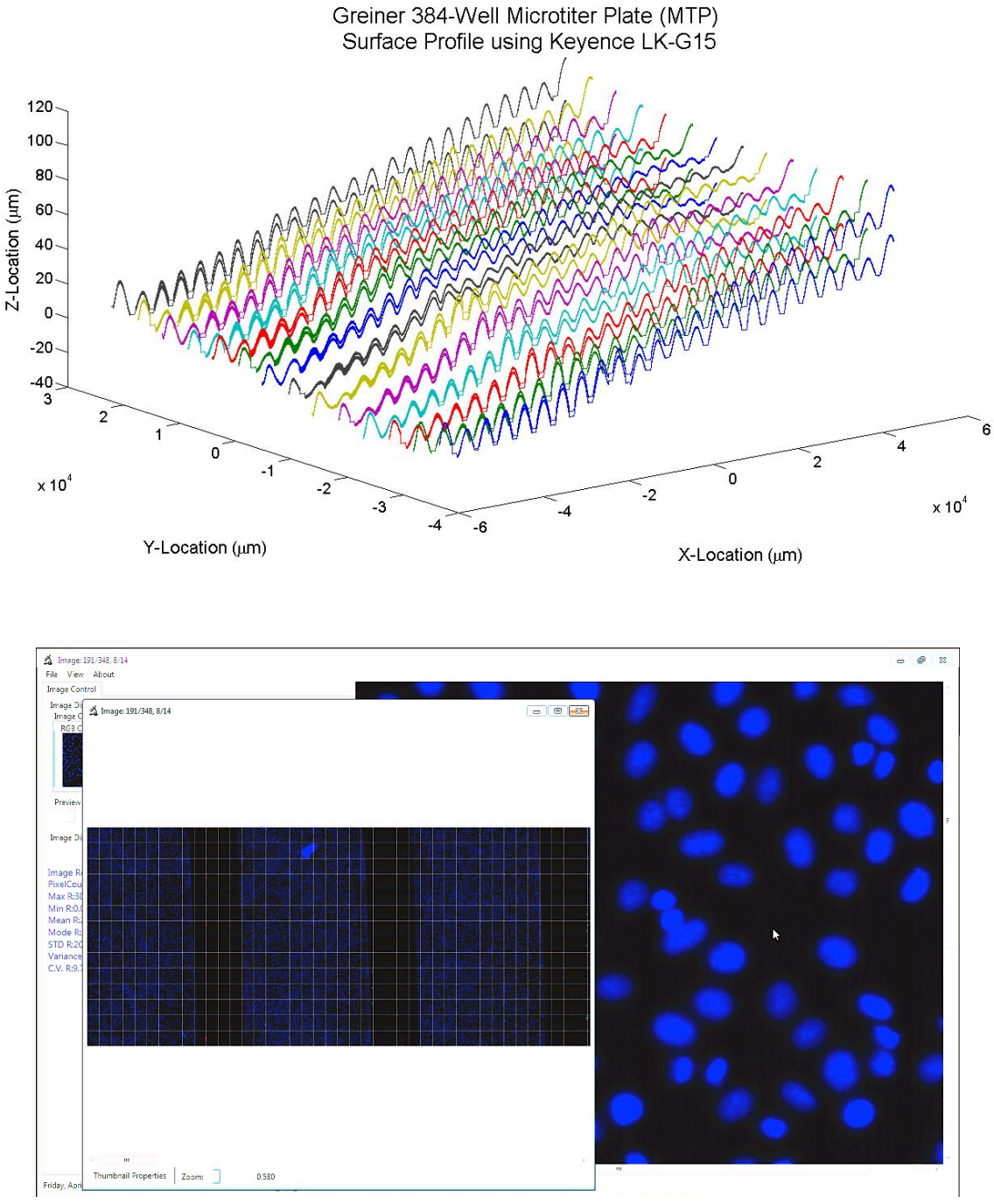

Figure 4.9: (a). Surface profile of the Greiner 384 well plate used for the PML assay as determined by the Keyence Sensor. (b). Screenshot of the custom TDI-CS capture and view software. The images are displaying the nuclear channel of the PML Oncogenic images stained with DAPI.

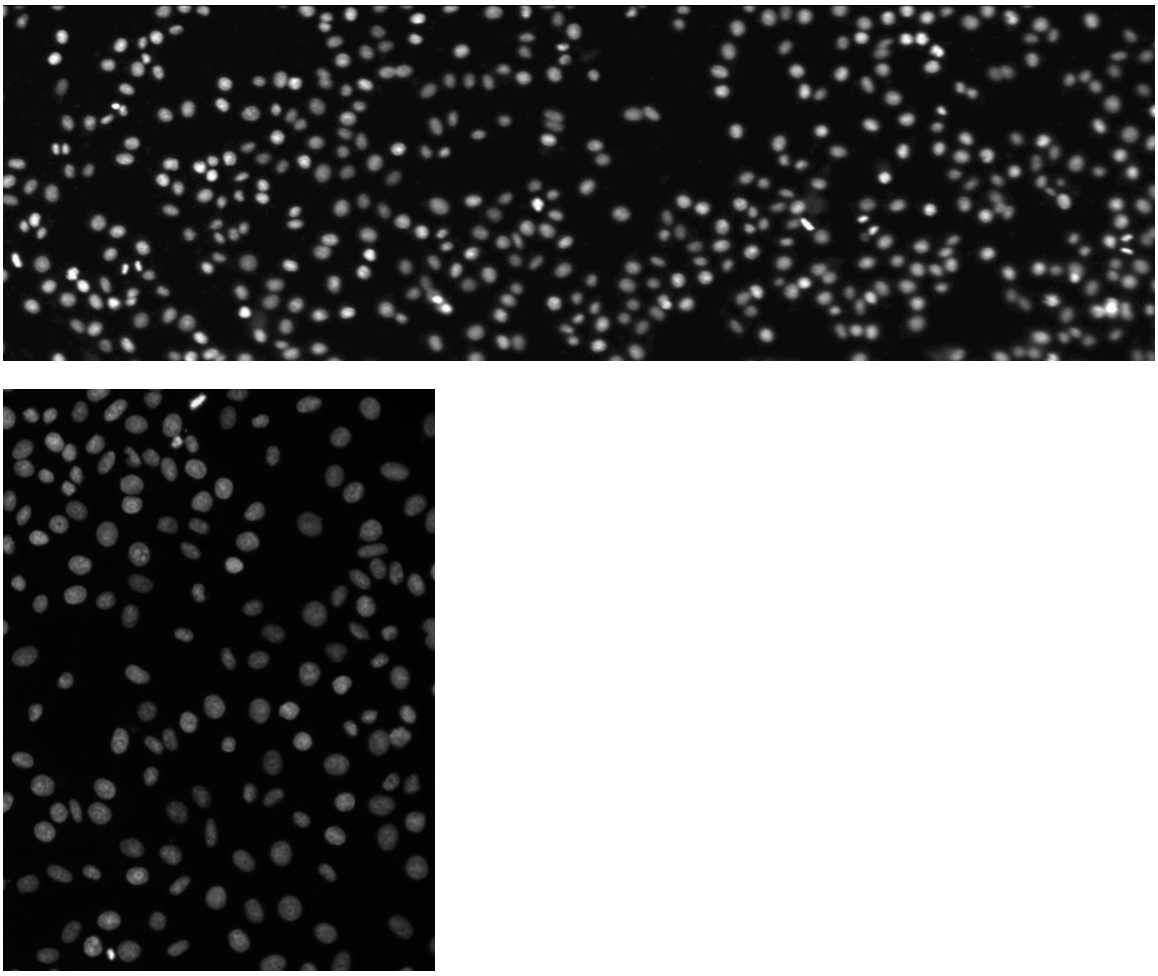

Figure 4.10: Images of the Nuclear channel of the PML Oncogenic Domain Assay. (a). Cropped image of an entire well captured using the TDI-CS system. Image was cropped for presentation purposes. (b). Image captured using the Perkin Elmer Opera.

For this experiment, the TDI-CS scanning parameters were similar to those used to scan the Ronchi Ruling Grid.

The PML plate was first scanned on the Perkin Elmer Opera and then scanned on the TDI-CS instrument. The parameters for scanning the plate on the Perkin Elmer Opera involved 2x2 binning and sampled 2 fields of view per well. The TDI-CS system scanned the same plate using 1x1 binning and scanned all available fields of view per well for the entire well plate. This automatically causes there to be more nuclei per image from the TDI-CS versus the Opera. The results measured by CyteSeer showed the nuclei of the cells in the images captured on the Opera had an average roundness of 1.21 ± 0.01μm. The nuclei of the cells captured on the TDI-CS images had an average roundness of 1.23 ± 0.02μm. There are approximately 7 images per well available in a 384-well dish at 20x magnification (excluding the edges of the well). Due to this, roughly 3.5 times the number of nuclei was interrogated to determine the roundness of the nuclei on the TDI-CS system vs. the Opera. The results of CyteSeer's analysis showed that the two image groups reported similar nuclear density (count per image) as well as a statistically similar measure of roundness. This analysis used a metric that is sensitive to focus and blur.

Chapter 5: Results & Conclusions

Using system specifications alone, we see that the performance bottleneck comes from the TDI camera itself when coupled with our optical setup. The top operating line rate of 8,000 Hz caps the maximum travel velocity of the stage. Using a de-magnification lens of 0.5375x or 0.2687x in place of the intermediate camera zoom of 1.075x would help increase the maximum travel velocity by a factor of 2 and 4 respectively. This addition to the optical train immediately brings the continuous scanning systems well count per day performance into the desired range. The trade-off however is the data per pixel information we are able to gather will be far from Nyquist given the NA of our objectives, 0.5 NA for the 10x and 0.75 NA for the 20x.

An alternative solution would be to use a faster line rate TDI camera. Increasing the line rate to a maximum of 16,000 Hz would also bring the continuous scanning systems well count per day performance into the desired range. The trade-off with an increased line rate however, is the decrease in the exposure time of each image. TDI imaging works by capturing microseconds worth of information at each vertical stage of a CCD. At each vertical line, more photoelectrons from the moving target are captured. This makes the effective exposure time a function of the number of vertical stages available as well as time spent at each stage. The vertical line rate governs this time. Increasing the line rate decreases the time spent. Commercially available TDI cameras have line rates of 10 KHz, 20 KHz, 50 KHz, and 100 KHz.

Another trade-off with fast line rate TDI cameras is the number of vertical stages available. The number of vertical lines available in TDI cameras is typically 64, 128, 256 or 512 lines. These numbers indicate the maximum exposure or integration time available for an image given a line rate of 20 KHz is 25.6 ms (assumes CCD with 512 vertical lines). Image exposure times on this time-scale are not suitable for low-light and epi-fluorescent microscopy. Typical exposure times are 4 to 8 times higher. In order to accommodate such low integration times, one must use a dedicated high power light sources to almost instantaneously excite and saturate fluorphores to ensure that there will be a bright enough signal for the CCD to detect at each integration stage. Another solution would be to use a TDI EM-CCD camera. EM-CCD, electron multiplying Charge Coupled Device, allows for high linear gain (up to 4000x) to be applied to the signal captured without adding noise associated with traditional gain. This imaging technique is well suited for high frame rate, low light imaging. At the time of hardware selection, TDI EM-CCD cameras were not commercially available. Hamamatsu now has a C9100-03 TDI camera that is well suited for continuous HCS. The C9100-03 is a 1000 (h) x 1000 (v) 1MP camera that has a pixel cell size of 8.0 μm^2 and a max vertical line rate of 31 kHz. The max gain associated with the camera is 2000x. Our C7780-51 TDI camera has a max gain of 5x. The C9100-03 at 20x magnification has 0.4 µm/pixel. Using a line rate of 30kHz gives us a stage velocity of 12mm/s. This is 5 times faster than the speed possible with

the C7780-51 TDI. Using the C9100-03, we would be able to scan over 130,000 wells per day or 388 plates in a 384-well format at 20x.

For the project, we decided to use a custom Hamamatsu CCD camera solution, the C7780-51 TDI, because it provided two of the three performance requirements:

- ✓ The ability to capture 3 channels simultaneously with independent gain control.
- ✓ Large number of integration stages to improve low-light imaging (1024).
- × Fast line rate of 20KHz to 50KHz.

Although the C7780-51 TDI does not have the appropriate line rate to let us hit our wells per plate milestone, we see that as CCD technology improves having a camera that can have a large number of integration stages, a fast line rate, have very low noise and high gain (EMCCD or ICCD), and multiple CCDs (3 to 5 CCD) is not far off and is simply a matter of custom fabrication. Due to this, we used the C7780-51 as our proof-of-concept camera to show that 3 channel TDI used in concert with dynamic autofocus could enable the capture of in-focus images much faster than traditional HCS techniques.

The Keyence laser displacement sensor is able to reliably track the surface contours of membranes of microtiter well plates. However, using the sensor in a position offset from the optical axis requires pre-calibration in order to

ensure a 1:1 mapping of displacement information with respect to X,Y coordinates. The reliance of the translation stage to have flat and straight travel is greatly increased as well. This would not be the case if the optical displacement measurement was performed through the objective or in line with the optical axis.

A linear encoder resolution of 1nm to 100nm is adequate for use to provide the TTL pulse train required to drive and synchronize a TDI camera to the travel of a moving object (depending on the desired line rate). Having the proper electronics to divide or parse the raw signal of the encoder and convert it to a phase locked, noise free (spurious peaks and inherent electronic noise removed), smooth and continuous pulse train is essential to work within the limits of the TDI CCD camera.

Using C#, the latest generation computing and data storage technology, and modern software development motifs it is possible to create a stand-alone workstation capable of driving and recording large volumes of high-bandwidth HCS data. Further development can allow real-time data processing to bring the true time associated with an HCS screen to only rely on the data acquisition and plate handling time.

The Ronchi Ruling grid as a synthetic target for determining focus and resolution performance of the TDI system showed that a high throughput, high bandwidth HCS system using Time, Delay and Integrate CCD imaging and dynamic autofocus is possible. The mechanics and setup needed to have optimal

performance for flat uniform substrates requires pre-calibration of the system and can potentially need a displacement look-up table (calibration correction factor) depending on if the equipment used is subject to cantilever or roll during stage movement. Flat substrates will have better repeatability over large scans.

The PML oncogenic domain assay from the SBCCG, allowed for the direct comparison of the TDI-CS system versus a gold standard HCS machine. Using a "real-world" assay showed the simplicity, elegance and necessity to use a high bandwidth data acquisition format. Using nuclear feature analysis to compare images captured on both systems, the TDI-CS system showed similar results. This is basic proof of concept and requires further testing on a larger data set(s) to truly verify performance.

Time delay and Integrate CCD image capture of HCS data using continuous stage motion and dynamic autofocus has been demonstrated to reduce equivalent scan times by 4x and collect 5 times as much data with this research. With optimized equipment (faster line rate and more sensitive >70% Q.E. TDI camera, flat and straight travel stage with constant velocity, and a through the objective or co-axial with the optical axis laser displacement) and flat bottom micro titer well plates (cyclic olefin polymer or glass bottom), the TDI-CS system has potential to allow for the increase in wells scanned per day for an HCS screen to more than 350,000 wells per day. This would bring image based high content screening into the ultra-high throughput regime.

Chapter 6: Additional Work

The primary goal of the TDI-CS project was to develop an instrument capable of increasing the bandwidth of data collection for HCS. To accomplish this, a system was put together and tested against a commercially available HCS machine. Additional work performed by other graduate and post-doctoral researchers in the Price Lab aided in helping to understand how to properly quantify how changes in optical focus effect image resolution as well as downstream assay analysis.

The following descriptions and figures are adaptations of work performed by Behrad Azimi, Ramses Agustin, Derek Fuller, and Mirco Guigli.

Depth of Field Out of Focus Distances

	20X 0.75 NA Objective		20X 0.5 NA Objective	
	1.0X Tube Lens	1.5X Tube Lens	1.0X Tube Lens	1.5X Tube Lens
Depth of Field (μm)[a]	1.23 μm	1.04 μm	2.66 μm	2.43 μm
Resolution Loss (%)	21%	23%	29%	34%
Distances from Focus	-0.6, 0.63 μm	-0.44, 0.6 μm	-1.38, 1.28 μm	-1.4, 1.03 μm

[a]Eq. 2.18 in Inoue and Spring, 1997

$$d_{tot} = \frac{\lambda_0 n}{NA^2} + \frac{n}{MNA} e$$

Through-Focus Images of DAPI-labeled NIH 3T3 Cell Nuclei (20X Objective)

Defocus: *1.0X Tube Lens (45x45-μm^2 regions; sampling of 0.323 x 0.323 μm^2/pixel)*

-3.0 μm -2.0 μm -1.0 μm 0.0 μm +1.0 μm +2.0 μm +3.0 μm

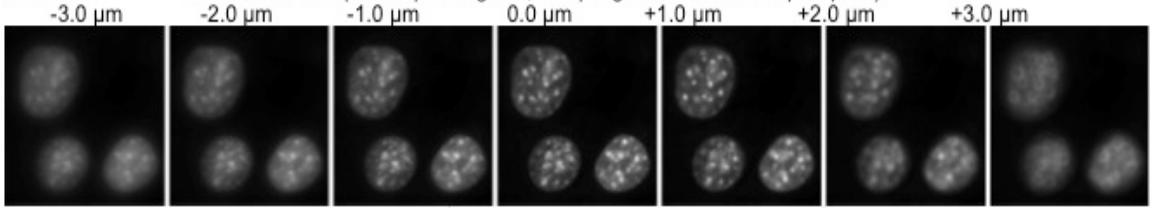

Figure 6.1: (a). Chart comparing resolution loss as a function of tube lens power and defocus distance. (b). Image compilation of NIH 3T3 cells.

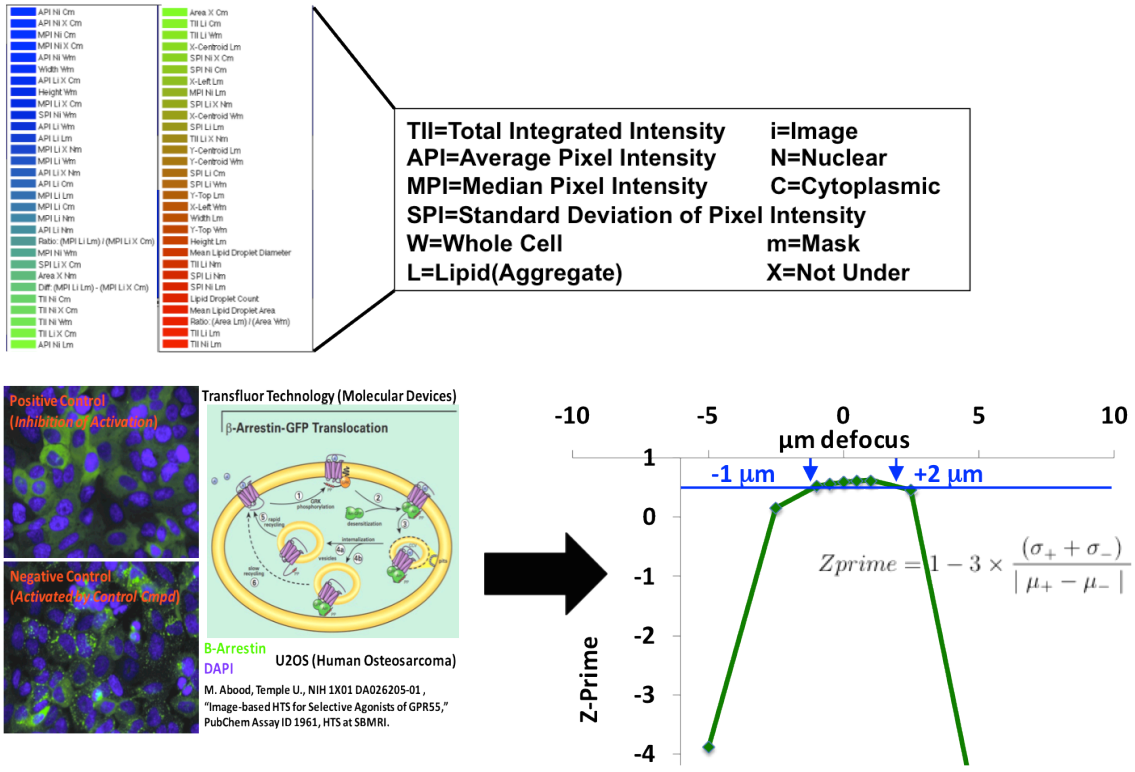

Figure 6.2: Measurements sensitivities (top right) are shown vs. defocus for the b-arrestin-eGFP (green) translocation assay (lower left). The CVs of the most sensitive features (ordered blue for most and red for least sensitive, upper and middle right) degrade within ± 1 mm; they are very sensitive to defocus. Z' (Zprime) ≥ 0.5 is the key test for assay validation for a primary screening campaign (now against 350,000 compounds in the NIH library). For this assay, which is based on the per cell count of vesicles (green, lower left image), Z' degrades below 0.5 outside a defocus range of -1 to +2 mm.

6.1 Focus and the Z-Prime Score

As mentioned previously in the introduction, the Z-prime score is a metric used to determine the value of performing a High Content Screen. Because of the costs and prep time associated with large screens, a metric that can quickly determine the validity of performing the desired screen is essential.

The impact of focus for a Z-Prime score was the subject of research for Drs. Azimi and Fuller. In their research, they discovered that certain features are focus sensitive and focus insensitive. Features such as total integrated intensity (integrated pixel intensity over a region of interest area) and whole cell dimensions (area, circumference, roundness) are extremely focus sensitive. Their work helped determine the roundness metric for the cells nuclei was one of the best features to compare the TDI-CS system versus the Opera.

6.2 TDI Camera Comparison

The only camera used for the experiments was the Hamamatsu C7780-51 TDI. As a result, all data generated by the system was greatly influenced by the performance of the C7780-51. It was hypothesized that the loss in resolution found with the Ronchi Ruling grid experiments was due to motion blur because of mismatch between line rate and stage velocity. In order to thoroughly test this, another camera from Hamamatsu was used while keeping the remaining components of the TDI-CS system the same.

For the camera comparison, the replacement camera for the C7780-51 was the C10000-401. This camera has a 2048 pixel horizontal and 128 pixel vertical resolution. The maximum line rate for the camera is 50kHz and the TDI capture is performed across the 128 vertical integration stages. The camera is back-thinned, is capable of bi-directional TDI mode, has a square pixel size of 12um x 12um, and has 4-tap TDI output. The 4-tap output refers to how the

horizontal pixel information is digitized and read off the camera. The 4 taps breaks up the 2048 horizontal resolution of the C10000-401 into 4 regions of 512 pixels. Each section is read simultaneously. The C7780-51, which has a 1344 pixel horizontal resolution, only has 1 tap.

Experiments we're performed using the Ronchi Ruling grid to compare the difference in reported resolution for the C7780-51 and the C10000-401 under similar optical conditions. Due the difference in maximum line-rate for the C10000-401, a comparison between resolution and line rate was also performed.

The results of the comparison are presented in a series of charts and graphs shown below:

Table 6.1: Comparison of resolution and line rate for the Hamamatsu C7780-51 and the C10000-401

Camera	Camera Mode	Frequency [kHz]	Stage Velocity [mm/s]	Image Count	Light Power	Light Power %	Gain	Resolution [pixel]	STD [Pixel]	Resolution [um]	STD [um]
C10000-401	TDI	1	0.3	2655	110	43	0	5.55	0.30	1.6655	0.089
C10000-401	TDI	5	1.5	2650	175	69	0	5.95	0.39	1.7862	0.1165
C10000-401	TDI	10	3	2646	220	86	0	5.69	0.43	1.7075	0.1299
C10000-401	TDI	15	4.5	2641	235	92	0	5.32	0.19	1.5965	0.0563
C10000-401	TDI	20	6	2637	230	90	2	5.48	0.31	1.645	0.0939
C10000-401	TDI	25	7.5	2624	230	90	4	5.55	0.58	1.666	0.1736
C10000-401	TDI	30	9	2627	250	98	4	6.15	1.12	1.845	0.3348
C10000-401	TDI	35	10.5	2622	250	98	5	7.23	2.47	2.17	0.7395
C10000-401	TDI	40	12	2616	250	98	6	8.03	3.47	2.41	1.04
C7780-51	Area	-	-	101	237	93	0	4.8	0.113	1.44	0.034
C7780-51	TDI	6	1.8	331	237	93	0	7.667	1.267	2.3	0.38

From the Ronchi ruling comparison, it is seen that there is a clear difference between the resolution of the C7780-51 and the C10000-401. Resolution appears to also be a function of line rate with the C10000-401. Faster line rates tend to cause increased degradation in resolution. This could be attributed to unstable electronics within the camera at the higher line rates, non-constant velocity of the translation stage, or reduced exposure time per frame.

With the comparison of the C7780-51 and the C10000-401, it is seen that there is a significant difference between Ronchi Ruling image resolution. The stage, linear encoder, and other timing components were not changed between the two experiments and the C7780-51 performed much worse under all conditions. This leads us to believe that the C7780-51 may not have been the right camera to develop the prototype TDI-CS instrument. Using the C10000-401, the graduate student working on the project, Mirco Guigli, has found that the Ludl stepper motor is able to provide proper velocity matching with the TDI camera even when using a pure TTL square wave provided from a function generator.

References

1. Giuliano, K. A., DeBiasio, R. L., Dunlay, R. T., et al. High Content screening: a new approach to easing key bottlenecks in the drug discovery process. J. Biomol. Screen 2, 249–259. 1997

2. Taylor D, Giuliano K. Mutiplexed high content screening assays create a systems cell biology approach to drug discovery. Drug Discov. Today 2, 149 154. 2005

3. Souchier C, Brisson C, Batteux B, Robert-Nicoud M, and Bryon PA. Data reproducibility in fluorescence image analysis. Methods Cell Sci. 25, 195–200. 2003

4. Gough AH, Johnston PA. Requirements, Features, and Performance of High Content Screening Platforms. Methods in Molecular Biology, Volume 356, II, 41-61. 2006

5. Origins of TDI - Sarnoff Corporation: http://sarnoff.com/research-and development/imaging-solutions/time-delay-integration

6. Piston D.W. Choosing objective lenses: the importance of numerical aperture and magnification in digital optical microscopy. Biol. Bull. 195, 1–4. 1998

7. Liron Y, Paran Y, Zatorsky NG, Geiger B, Kam Z. Laser autofocusing system for high- resolution cell biological imaging. J Microsc;221(Part 2):145–151. 2006

8. Manian BS, Heffelfinger DM, Goldberg EM. Optical autofocus for use with microti- ter plates. 2002. U.S. patent #6130745.

9. Groen FC, Young IT, Ligthart G. A comparison of different focus functions for use in autofocus algorithms. Cytometry;6:81–91. 1985

10. Bravo-Zanoguera M, Massenbach B, Kellner A, Price J. High-performance autofocus circuit for biological microscopy. Rev Sci Instrum;69:3966–3977. 1998

11. Price JH, Gough DA. Comparison of phase-contrast and fluorescence digital autofo- cus for scanning microscopy. Cytometry;16:283–297. 1994

12. Oliva MA, Bravo-Zanoguera M, Price JH. Filtering out contrast reversals for microscopy autofocus. Appl Opt;38:638–646. 1999

13. Bravo-Zanoguera ME. Autofocus for High Speed Scanning in Image Cytometry [Ph.D. Dissertation], San Diego:University of California; 202 p. 2001

14. Bravo-Zanoguera ME, Laris CA, Nguyen LK, Oliva M, Price JH. Dynamic autofocus for continuous-scanning time-delay-and-integration image acquisition in automated microscopy. J Biomed Opt;12:34011. 2007

15. Soldatov, V. P. An analysis of images of rapidly traveling objects by means of optoelectronic devices. MEASUREMENT TECHNIQUES Volume 52, Number 9, 918-923. 2009

16. Chamberlain S. G, Jenkins P. T. Capturing images at 1000 feet per second with TDI. Photonics Spectra, No. 1. 1990.

17. Wong HS, Yao YL, Schlig ES. TDI charge-coupled devices: Design and applications. IBM Journal of Research and Development Issue Date: Jan. Volume: 36 Issue:1 83-106. 1992

18. Gilmore J, Bulayev Y. CCD advances improve TDI imaging techniques. Laser Focus World; 43(1):113-116. 2007

19. Miguel E. Bravo-Zanoguera, Casey A. Laris, Lam K. Nguyen, Mike Oliva and Jeffrey H. Price, "Dynamic autofocus for continuous-scanning time-delay-and integration image acquisition in automated microscopy", J. Biomed. Opt. 12, 034011 (Jun 11, 2007)

20. Lambert, B. M., & Harbold, J. M. (2009). Experimental methods for measurement of the modulation transfer function (MTF) for time-delay-and integrate (TDI) charge coupled device (CCD) image sensors. *Proceedings of SPIE*, *7405*(Ccd), 74050M-74050M-19

21. Scholtens, T. M., Schreuder, F., Ligthart, S. T., Swennenhuis, J. F., Tibbe, A. G. J., Greve, J., & Terstappen, L. W. M. M. (2011). CellTracks TDI: An image cytometer for cell characterization. *Cytometry Part A*, *79A*(3), 203-213.

22. Wong HS,Yao YL,Sclilig ES. TDI charge coupled devices: design and applications. *IBM J Res Dev* 1992; **36**:83: 106.

23. NanoZoomer Digital Pathology System C9600, sales.hamamatsu.com/assets/pdf/hpspdf/NDP.pdf 2006.

24. Ronchi Ruling: http://en.wikipedia.org/wiki/Ronchi_Ruling

25. Boone JM, Seibert JA. An analytical edge spread function model for computer fitting and subsequent calculation of the LSF and MTF. Med Phys; 21:1541-1545. 1994

26. Liron, Y., Paran, Y., Zatorsky, N. G., Geiger, B., & Kam, Z. (2006). Laser autofocusing system for high-resolution cell. *Journal of Microscopy*, *221*(August 2005), 145-151.

27. Wang, D.-J., & Zhang, T. (2011). Noise analysis and measurement of time delay and integration charge coupled device. *Chinese Physics B*, *20*(8), 087202.

28. Hu, E. (2010). Speed mismatch error in the profile measurement of moving object by using TDI imaging system. *Technology*, *7656*(1), 76561W-76561W-6.

29. Inoué S, Spring KR. VideoMicroscopy: The Fundamentals, 2nd Ed. Plenum, NewYork 1997

30. Fantone S. Modulation-transfer-function testing provides a clear assessment of imaging system performance. Everything in Modulation. SPIE Newsroom 29 March 2004.

31. Optical Resolution: http://en.wikipedia.org/wiki/Optical_resolution

Section II - Kinectic Image Cytometry

Chapter 1: Introduction

Automated high content screens allow for a wealth of information to be gathered from a given experimental study. If the hardware and controlling software are present, researchers are able to fine-tune the hardware performance to directly match their experimental needs. Unfortunately this is not always the case and scientists are forced to either tweak their experimental design or are required to build “in-house” tools to conduct their experiments. It was with this that we decided to develop a cytometry module that can be added on to existing HCS systems that is capable of stimulating and monitoring events that are sensitive to changes in action potential.

As a case study for this cytometry module, I decided to use calcium transient activity in neonatal rat ventricular myocytes (NRVMs). It has been shown that NRVMs exhibit calcium transients and contractile characteristics quite similar to embryonic stem cell-derived cardiomyocytes (ESCMs). Because of this, using NRVMs as a test-bed for this add-on module will ensure that researchers interested in exploring the effects of various chemical compounds and genes on ECSMs will be able to do so in the context of HCS.

Chapter 2: Research Summary

For the Kinetic Image Cytometry project, I developed a module that can be easily integrated into current HCS Instruments (Beckman Coulter: IC-100 and GE Amersham: In-Cell 1000) that is capable of automatically stimulating and monitoring calcium transients in NRVMs Cardiac Myocytes, developed / incorporated image processing algorithms that will automatically segment individual cardiac cells and quantify calcium transients on a cell-by-cell basis, and validated and characterized the systems performance using dose response assays to test systems ability to track changes in cardiac myocyte calcium transients.

Chapter 3: Publication

The following describes a complete look into the work done to develop and use the Kinetic Image Cytometrer (KIC) to monitor calcium kinetics in neo-natal rat ventricular myocytes (NRVMs). The section discusses the development of the system and testing using NRVMs. The goal was to quickly build the KIC around an existing high content screening (HCS) instrument and ensure that the system was able to accurately track calcium transients in NRVMs under normal settings and with a dosage response assay using dynamic kinetic monitoring and post capture automated cell by cell segmentation and analysis.

3.1 AUTOMATED CALCIUM MEASUREMENTS IN LIVE CARDIOMYOCYTES

3.1.1 Background and Significance

Heart failure due to hypertension, infarction, or other factors, is a leading killer of men and women in modern society and involves, at its base, a debilitating loss of cardiomyocytes. Recent studies indicate the feasibility of regenerating lost cardiomyocytes by transplanting embryonic stem cell-derived cardiomyocytes (ESCMs) or mobilizing resident stem cells. To realize the potential of stem-cell based therapies, we hypothesize that it will be extremely beneficial to develop technology and instruments for high throughput, high content screening (HCS) of drugs and genes for their ability to stimulate the formation of functional, contractile cardiomyocytes. Contractile activity is the primary physiological function of cardiomyocytes and abnormal contractility is potentially lethal. We discuss the first phase of the development of an instrument dedicated to distinguishing differentiated ESCMs from undifferentiated non-cardiac background cells using automated cell-by-cell quantification of contractile-calcium transients as the primary assay.

The contractile cycle of cardiomyocytes is divided into an abrupt shortening phase (systole), induced by a rapid rise in the intracellular calcium concentration ($[Ca^{2+}]_i$) due to calcium entry via voltage dependent L-type calcium channels and calcium-induced-calcium release from the sarcoplasmic reticulum (SR). Contraction is followed by relaxation of the cell (diastole) and the decline of

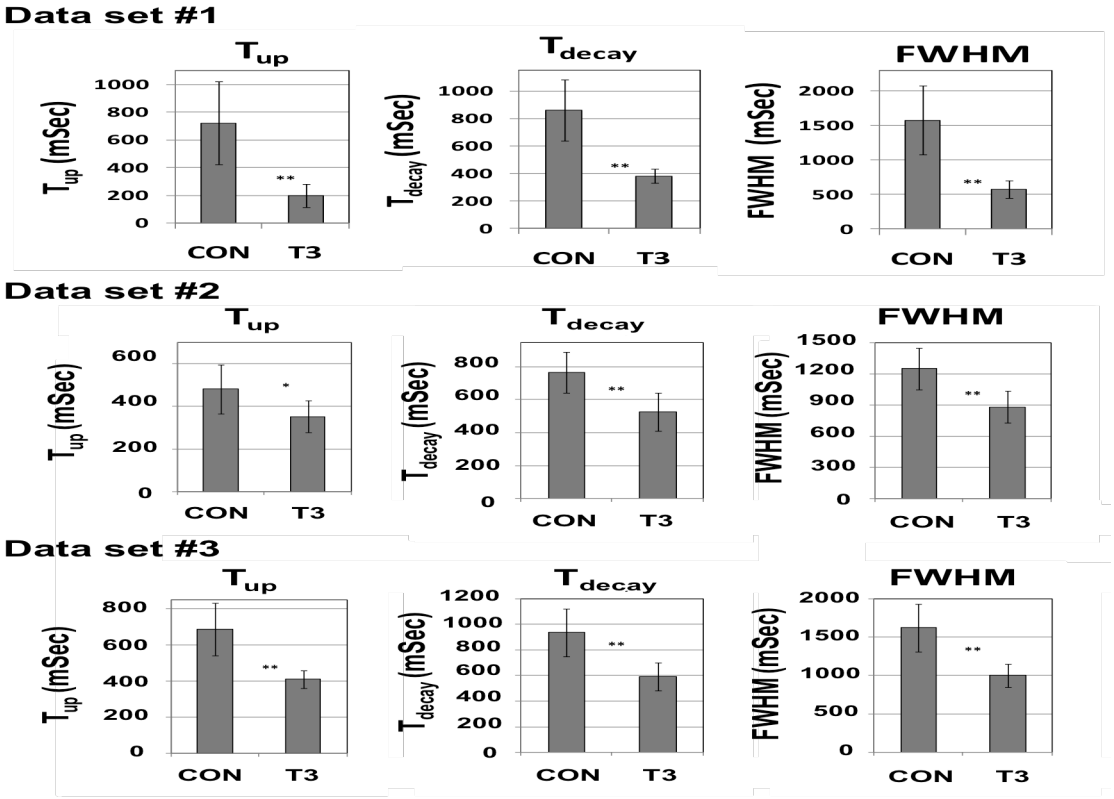

Figure 3.1: Effect of thyroid hormone (T3) on contractile calcium kinetics in NRVMs measured by automated microscopy and image analysis. Each bar represents the mean ± SD for n= 8 wells for control cells or n= 12 to 22 wells for T3-treated cells. An average of 110 cells were measured, per well. The experiment was repeated with 3 different preparations of NRVMs which were analyzed independently (data sets 1, 2, and 3).

$[Ca^{2+}]_i$. Decline of $[Ca^{2+}]_I$ during diastole is controlled primarily by re-sequestration of calcium back into the SR by SERCA2, an ATPase associated with the SR membrane.

Calcium transients have been recorded from cardiomyocytes derived from embryonic stem cells (both from mouse and from human) by several laboratories. For example, calcium transients in fura-2-loaded cardiomyocytes derived from human embryonic stem cells (hESC-CM), were observed in spontaneously contracting embryoid bodies[1]. hESC-CMs cultured on mouse visceral-endoderm

like cells showed similar calcium transients and spontaneous contractions at 0.6 to 1.5 Hz[2]. Fluo-4 has been used to record calcium transients from murine ESCMs, which exhibited spontaneous contraction rates of approximately 1 Hz[3]. Consistent with the wide spread observation of spontaneous beating in experiments designed to elicit the appearance of ESCMs, myocytes with “pace-maker” activity have been observed in contracting cell clusters, serving to drive the contractions of neighboring cells[5,6]. These studies indicate that ESCMs typically exhibit calcium transients and contractile characteristics similar to neonatal rat ventricular myocytes (NRVMs), rather than adult ventricular cardiomyocytes. Thus, for our experimentation we used NRVMs as a test-bed to develop our instrument.

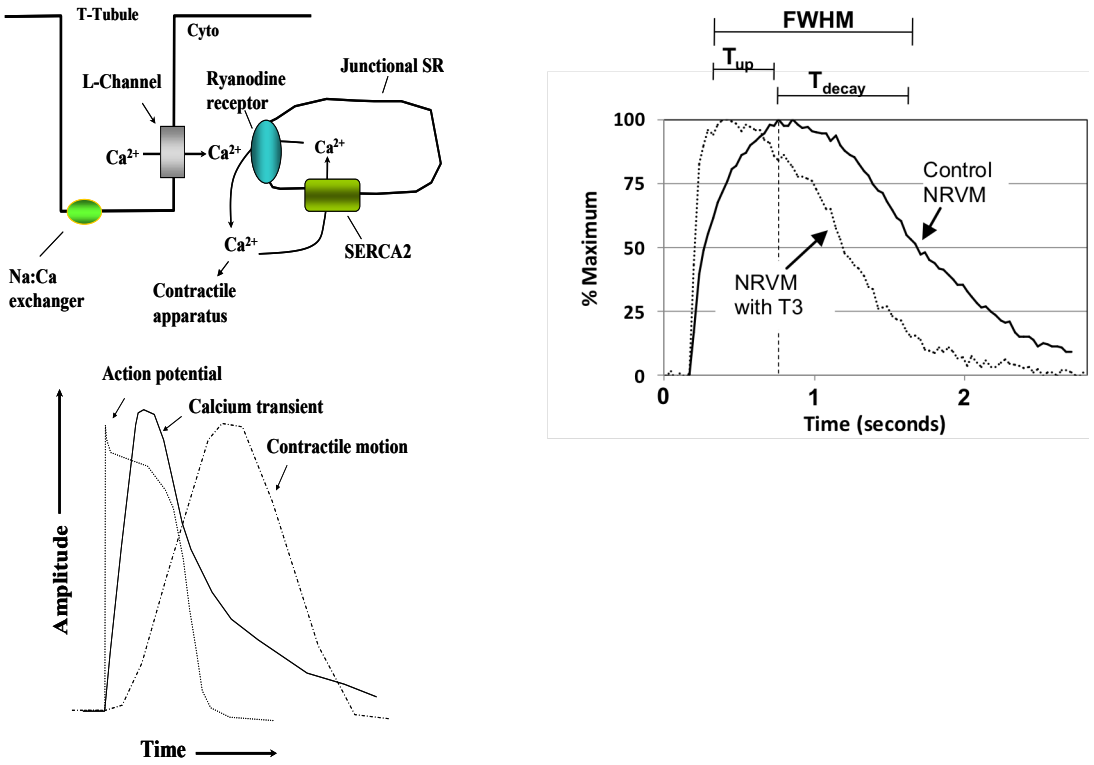

Figure 3.2: (left) The cardiac contractile cycle[7] (adapted from Bers 2002).A) Calcium-induced calcium release from the SR and the role of SERCA2 to reuptake Ca^{++} into the SR. B) The cardiac action potential, calcium transient and myocyte contraction. (right) Parameters for quantification of contractile calcium kinetics are shown. The transients are for a control NRVM (solid line) and for a NRVM maintained in 100-nM thyroid hormone (dotted line) normalized to their minimum (0%) and maximum values (100%). The kinetic parameters derived from the transients are the Full Width at Half Max (FWHM) which is the time required for progression from the 50% point on the upstroke to 50% point on the downstroke, T_{up}, which is the time from the 50% point to 100% on the upstroke, and T_{decay}, which is the time period from the 100% point to the 50% point on the decay phase.

Automated high content screens allow for a wealth of information to be gathered from a given experimental study. If the hardware and controlling software are present, researchers are able to fine-tune the hardware performance to directly match their experimental needs. Unfortunately, this is not always the case and researchers are usually forced to either tweak their experimental design or are required to build “in-house” tools to conduct their experiments. With this in mind, our goal was to develop instrumentation and

software for cell-by-cell recording of Ca^{2+} transients that is easily integrated into current laboratory setups. This module (the Kinetic Image Cytometer, or KIC) will interface easily to commercially available high content microscopy workstations, which already perform plate scanning and image acquisition, to enable video burst acquisition and analysis of calcium transients in a fully automated (high throughput screening) mode. The KIC will electrically stimulate (or pace) the cells, record the resulting Ca^{2+} transients from cells in microtiter plates (e.g., with 96 wells), and automatically quantify characteristics such as the duration of the Ca^{2+} waves on a cell-by-cell basis in a fully automated manner on large scale screens (e.g., tens to hundreds of thousands of compounds).

3.1.2 Materials and Methods

The KIC module was interfaced with an existing high content screening system, the EIDAQ 100 (Q3DM, San Diego, CA). The EIDAQ 100 is functionally identical to (i.e., utilizes the exact same hardware and controlling software, CytoShop, as) the later-released Beckman Coulter IC 100. Q3DM sold the EIDAQ technology to Beckman Coulter in December 2003 for manufacturing and worldwide distribution.

The EIDAQ 100 includes: 1) an inverted epifluorescence microscope (Nikon Eclipse TE2000-U), 2) an intensity- feedback stabilized 100 W Hg arc lamp developed by Q3DM, 3) excitation and emission filter wheels, 4) a motorized stage with XY-axes control, and 5) a piezoelectric *Z*-axis control for fast, precise autofocus. A Nikon multimode module to the autofocus and

scientific grade CCD cameras splits the emission light path on the EIDAQ 100. The EIDAQ 100's scientific grade camera was removed from the optical path but left powered on and connected to allow normal CytoShop operation.

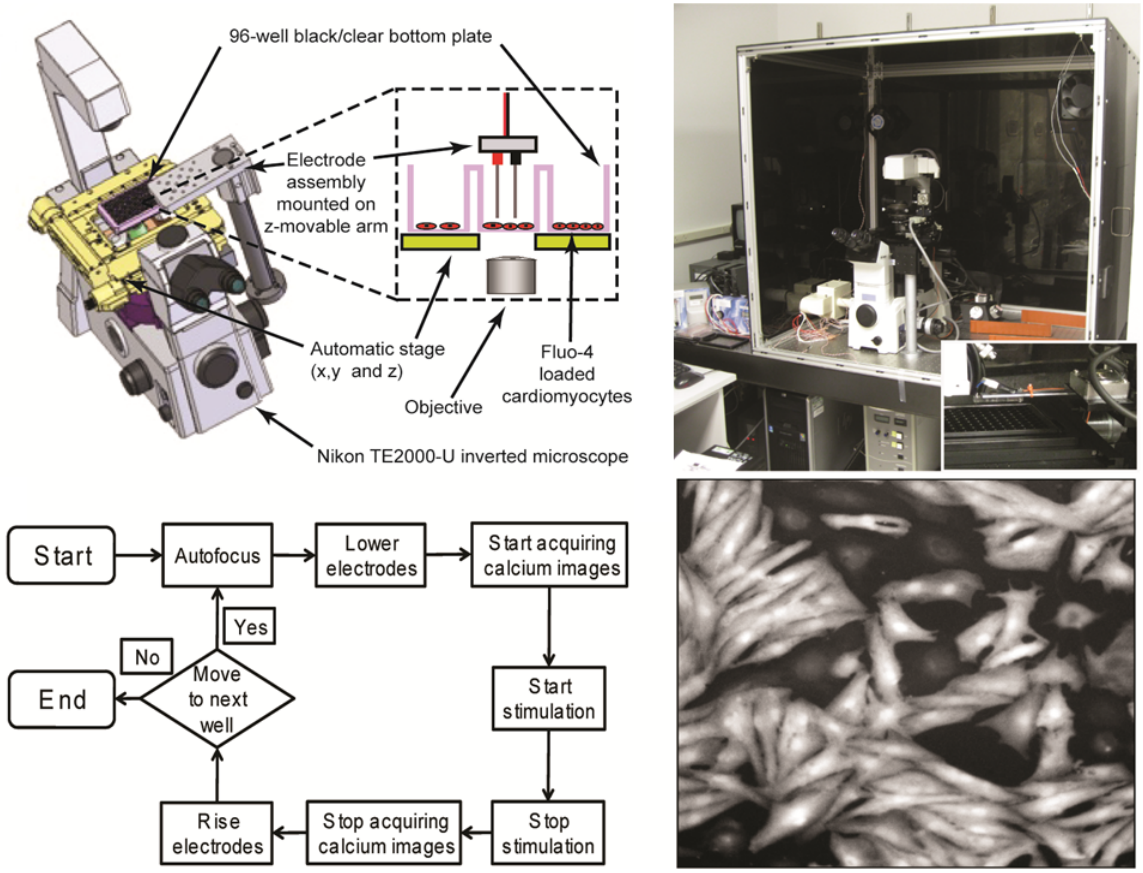

Figure 3.3: Schematic showing KIC system and workflow.

KIC Instrumentation Module.

The components of the KIC module include a separate PC running Windows XP and control software programmed in Labview 8.0, (National Instruments, Austin, TX), a National Instruments data acquisition I/O board, the NI-PCI-6251, a stimulator/electrode assembly (lowered and raised using a computer-controlled Sutter Instruments (Novato, CA) micromanipulator, the MP-

285), a Grass Technologies (West Warwick, RI) S48 square pulse stimulator, and a high speed scientific-grade CCD camera, the back-illuminated iXon DU-897 EMCCD from Andor (South Windsor, CT).

Data Acquisition. NVRM green channel video streams of 3-10 seconds at 30fps, comprising 1-3 electrical stimuli and triggered by the electrical signal to the arc lamp shutter on the EIDAQ 100, were collected and stored directly to the hard drive of the PC controlling the CTIC module. Prior to video stream acquisition, the EIDAQ 100 auto-focused on the nuclear channel of the NVRMs. All images were captured at a magnification of 20x 0.50 numerical aperture (NA) and a 1x intermediate camera zoom.

Cytometric Analysis of Time-Series Images. Image analysis was carried out to obtain cytometric data by using ImageJ (U. S. National Institutes of Health, Bethesda, Maryland, USA), Matlab (The MathWorks, Inc., Natick, MA) and CellProfiler (BROAD Institute, Cambrigde, MA). Image analysis featured averaging of images in the time-series, background subtraction, and automatic segmentation.

An average of the time-series green-fluorescence channel images was corrected for background using ImageJs “Rolling Ball” background subtraction algorithm[8]. This background corrected image was then automatically segmented using CellProfilers “IdentifyPrimaryAutomatic” algorithm[8], which performs watershed with local maxima as the tessellation centers. This automated segmentation typically resulted in very good agreement with cells segmented

manually. The resultant cytoplasmic mask was then applied to each time frame image to quantify single cell integrated fluorescence intensity.

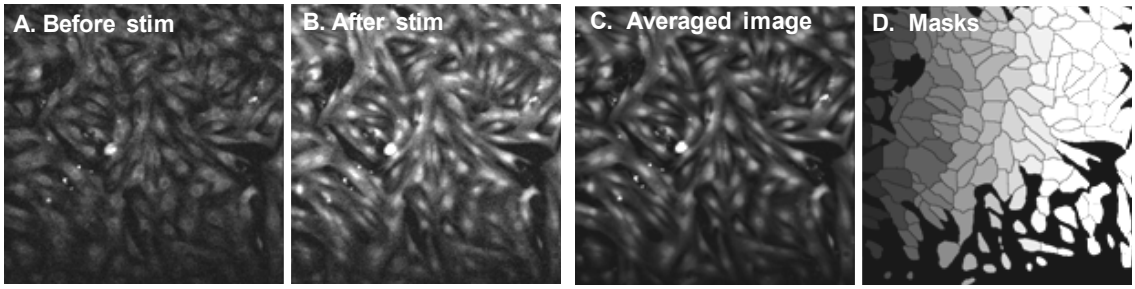

Figure 3.4: Strategy for segmentation of images derived from Flou-4 loaded cardiac myocytes A: A raw image of NRVMs prior to stimulation (low Ca^{++}, dim Fluo-4) is shown. B: The same field of view is shown immediately after electrical stimulation (high Ca^{++}. bright Fluo-4). C: The average of all images in the video stream. D: The masks segmented from the averaged image with each cell mask labeled by a unique gray-scale intensity.

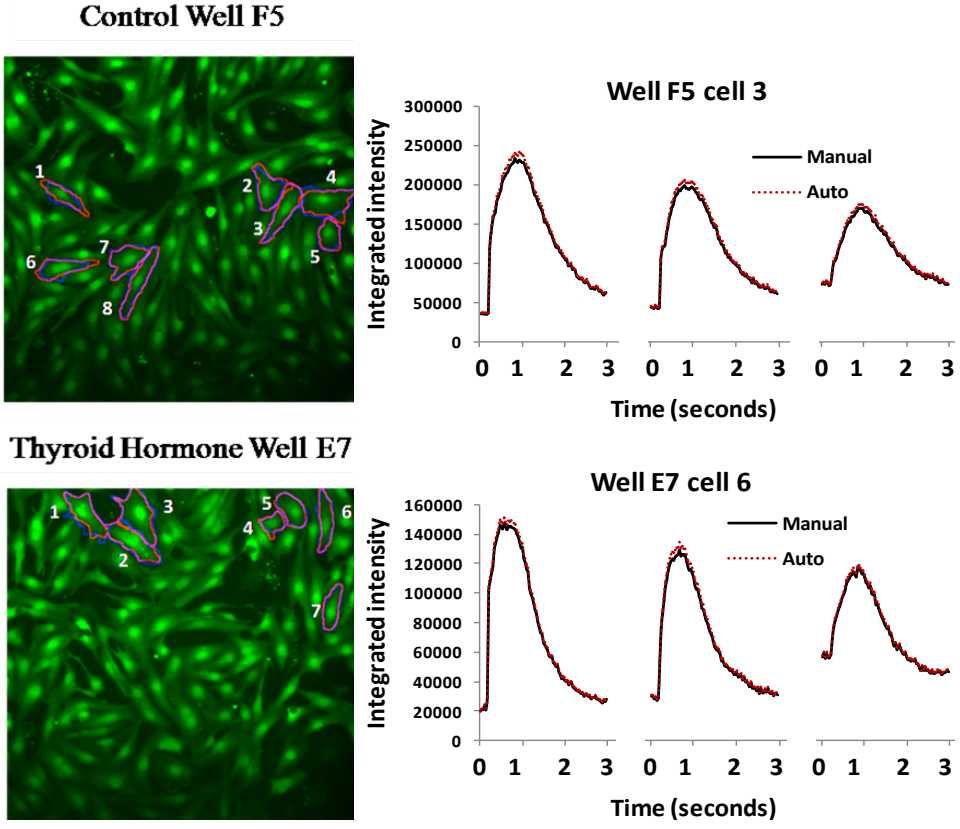

Figure 3.5: Manual vs. automated segmentation of images obtained from fluo-4 loaded NRVMs. *Upper,* Cell masks drawn manually (red) or via automatic segmentation (blue) are shown for cells cultured in control media; calcium transients are shown for cell #3 which was stimulated 3 times at 10 min intervals. *Lower,* Cell masks for cells cultured for 72 hr in 100 nM thyroid hormone; calcium transients are shown for cell #6.

3.1.3 Results and Conclusions

We report here the development of monitoring system capable of automatically recording and analyzing electrically stimulated calcium transients from cells exhibiting the phenotype of cardiac myocytes. Integration of the CTIC with the EIDAQ 100 was successfully achieved, and approximately 1300 video clips were obtained from electrically stimulated NRVMs. Cells cultured in thyroid hormone for 72 hr displayed markedly accelerated contractile calcium transients, as quantified by the automated methodology. For example, in a typical data set derived from over 2000 cells, T_{up}, T_{decay}, and FWHM were reduced by 73%, 56%, and 64%, respectively, by thyroid hormone. Furthermore, similar results were obtained for two additional experiments, performed on different preparations of NRVMs, which further illustrates the reproducibility of the effect of thyroid hormone on the NRVMs, and the consistency of the automated methodology..

Thus, the system can detect and quantify the effect of test compounds on the contractile phenotype of cells cultured under conditions very similar to those utilized in experiments designed to produce hESC-CMs. The apparatus could also be utilized to test for potential toxic or beneficial effects on fully differentiated cardiac myocytes, which may have applications for pharmaceutical screening and lead-compound characterization.

Chapter 4. Additional Work

Once the KIC system was developed, it was placed in the Sanford-Burnham Medical Research Institutes Stem Cell Research Center Core Facility. While there it was used as an instrument available to various graduate students, post-docs and research associates. This section shows a compilation of figures and tables from their respective work. Primarily Drs. Fabio Cerignoli, Pat McDonough, Ross Whittaker, and research associate, Piyush Gehalot,

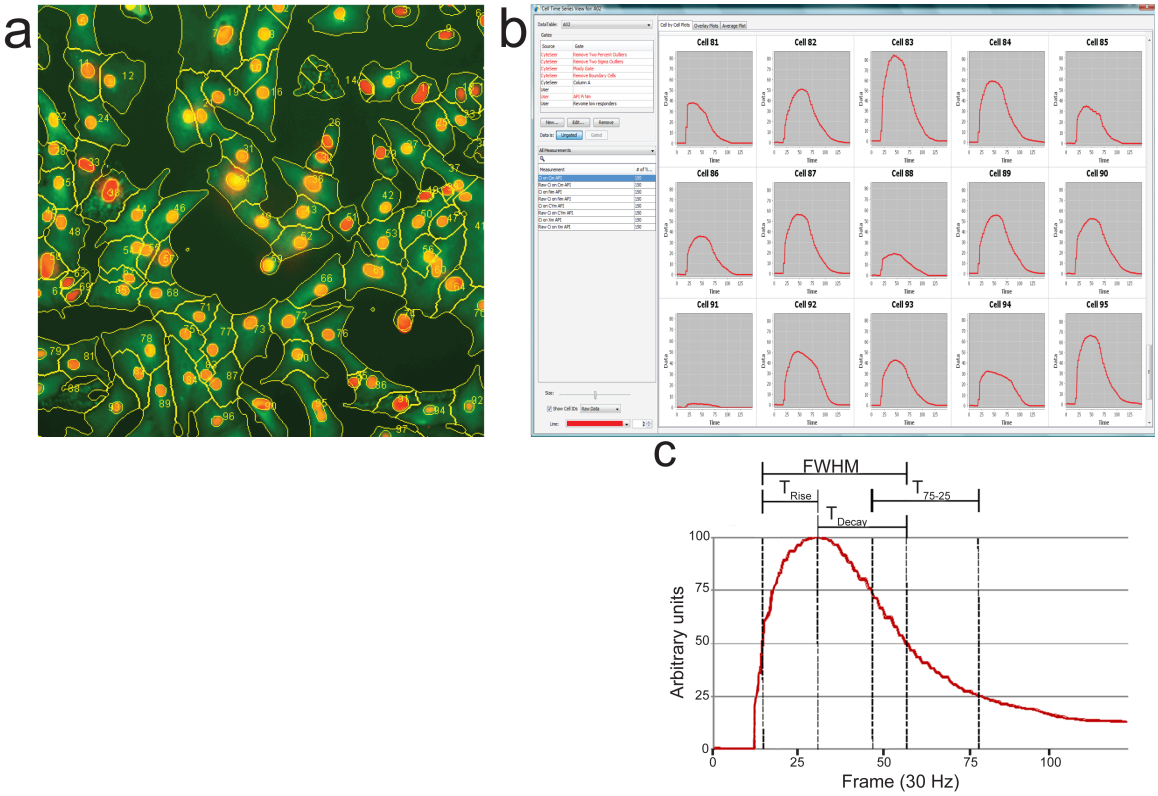

Figure 4.1: Image segmentation and single-cell Ca^{2+} analysis; (a). Cell nuclei (red), Ca^{2+} average signal (green) and cell boundaries (yellow) via CyteSeer on hiPSC-derived cardiomyocytes; (b). Screenshot of the software with single-cell Ca^{2+} traces plotted for some of the cells identified in (a); (c). Average Ca^{2+} transient curve with parameters that are automatically measured by the software.

performed the work.

The basic KIC hardware and software written during my research was expanded and added to commercially available software from Vala Sciences', Cyteseer. This software added automatic cell segmentation, quantification, and scoring of kinetic trace profiles. Figure 4.1 shows an example of the cell segmentation, the automatic trace identification and normalization, and trace scoring. The automated scoring looks at the T_{rise}, T_{decay}, $T_{25\text{-}75}$, and the full-width half-maxima (FWHM) profile of the time dependent transient wave. From this, the software can automatically gate out spurious cells, or sort cells based on anyone of these parameters.

With the automated scoring, the KIC system can now be used to better quantify dose response experiments. Table 4.1 reports the various chemical compounds used by Drs. Cerignoli, McDonough and Whittaker to perform does response assays to check abnormal contractility and calcium dynamics in NRVMs and hiPSCs. Figure 4.2 shows the work-flow of an experiment performed by Dr. Cerignoli where he paced a NRVM prep at a constant frequency to monitor the calcium recovery dynamics.

With the KIC system, a new world of research is made possible. The system is capable of detecting and quantifying the effects of test compounds on the contractile phenotype of cells cultured under conditions very similar to those utilized in experiments designed to produce hESC-CMs. The system can also

test for potentially toxic or beneficial effects on fully differentiated cardiac myocytes, which may have applications for pharmaceutical screening.

Table 4.1: Chart showing the various chemical compounds used in does response assays to check abnormal contractility and calcium dynamics in NRVMs and hiPSCs

	Lowest Effective Dose*			
	Spontaneous	1HZ	Reported IC50	Source
Verapamil	100 nM	1 uM	L-type- 0.6-3uM	1-4
BAY-K	10 nM	N/A	L-type-17.5 nM	5
Dofetilide	0.1 nM	1 nM	hERG-5-30 nM	6-10
NS1463	1 uM	N/A	hERG-10.5 uM	11
Flecainide	1 uM	1 uM	Na-600 nM	7,12
Levcromakalim	1 uM	N/A	490 nM	5
Sotalol	10 uM	10 uM	hERG-268uM	13
4-AP	1 uM	100 nM	I_{t0} 1.7 mM; $I_{k,sus}$ 29 uM	14
JNJ303	10 uM	100 nM	Ik_s-64nM	15
JNJ282	1 uM	1 uM	Ik_s-1.14 nM	15
Moxifloxacin	100 nM	N/A	29 uM	16
Lowest Dose Causing Statistically Relevant Abnormality*				

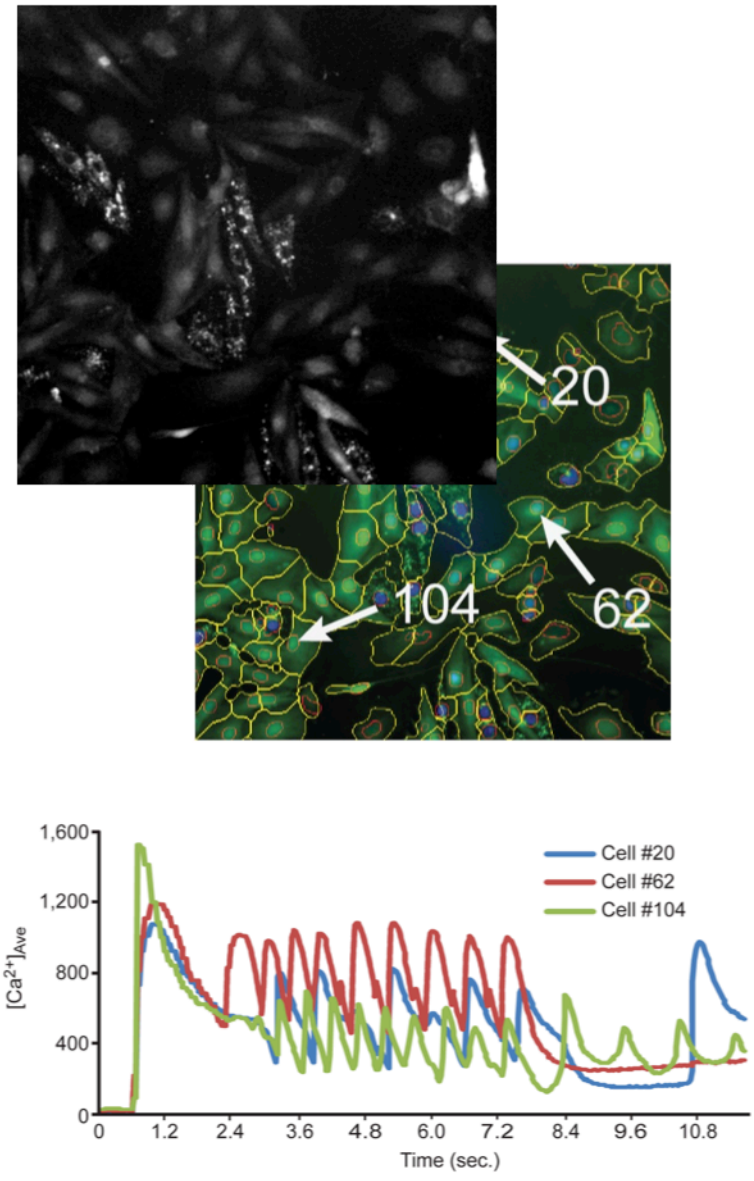

Figure 4.2: Schematic showing workflow from Fluo-4 loaded NRVMs to segmented calcium traces.

REFERENCES

1. K. Dolnikov, M. Shilkrut, N. Zeevi-Levin, A. Danon, S. Gerecht-Nir, J. Itskovitz-Eldor, O. Binah, “Functional Properties of Human Embryonic Stem Cell-Derived Cardiomyocytes,” *Ann. N.Y. Acad. Sci.* 1047, pp: 66–75, 2005.

2. Mummery et al., “Differentiation of Human Embryonic Stem Cells to Cardiomyocytes,” Circulation. 107, pp: 2733:2740, 2003

3. Grey, et al., “Fine-tuning in Ca^{2+} homeostasis underlies progression of cardiomyopathy in myocytes derived from genetically modified embryonic stem cells,” *Human Molecular Genetics* 14(10), pp: 1367-1377, 2005

4. Mery et al., “Initiation of Embryonic Cardiac Pacemaker Activity by Inositol 1,4,5-Trisphosphate–dependent Calcium Signaling,” *Mol Biol Cell*, 16(5), pp: 2414-23, 2005

5. Steven M. White and William C. Claycomb,“Embryonic stem cells form an organized, functional cardiac conduction system in vitro,” *Am J Physiol Heart Circ Physiol* 288, pp: H670-H679, 2005

6. S. R. Sternberg, "Biomedical image processing," IEEE Computer 16, pp: 22-34, 1983.

7. Donald M. Bers, “Cardiac excitation–contraction coupling,” *Nature*, Vol 415, pp: 198-205, 2002

8. Anne E. Carpenter et al., (2006) “CellProfiler: image analysis software for identifying and quantifying cell phenotypes,” Genome Biology, 7:R100, 2006